DRAG REDUCTION WITH POLYMER MIXTURES IN OIL-WATER FLOWS: EFFECT OF SYNERGY

Muhammad Muhammad Gimba[1], Lawrence Chukwuka Edomwonyi-Otu[1,2]*, Yusuf Nurudeen[3], Abdulkareem Abubakar[2]

[1]Department Chemical Engineering, Ahmadu Bello University, Zaria, Nigeria.
[2]Department of Chemical and Petroleum Engineering, Delta State University, Abraka, Nigeria.
[3]Department of Chemical and Petroleum Engineering, Bayero University, Kano, Nigeria.

*Corresponding author: uceclce@ucl.ac.uk +2349099265536, +2347085744312

Abstract: The pressure drop encountered during horizontal pipeline flows in chemical and petroleum industries require high pumping energy. It has been proven that frictional pressure drop in pipeline flows can be reduced by adding small amounts of high molecular weight polymeric solution. In this work, drag reduction (DR) in oil-water flows was investigated in 20 mm horizontal pipe diameter and length of 140 times the diameter (140*D). Partially hydrolysed polyacrylamide (HPAM), polyethylene oxide (PEO) and aloe vera mucilage (AVM) as well as their mixtures (HPAM+AVM and PEO+AVM) at mixture Reynolds number of 37773 were used. Master solution of 2000 ppm and 20000 ppm for HPAM, PEO and AVM as well as their respective mixtures at total concentration (tc) of 30 ppm and 400 ppm were used. The two liquids used were tap water (ρ = 0.997 g/mL, μ = 0.89 cP) and diesel oil (ρ = 0.832 g/mL, μ = 1.66 cP) at ambient conditions (25 °C, 1 atm). Different oil input volume fractions (βo) and mixture velocities (Umix) for the two phases were used. Maximum DR of 61.67 & 63.33%, and 66.67 & 68.33% were obtained for HPAM+AVM and PEO+AVM respectively, at mixing ratios of 3:1 & 1:19, for 25% oil input and water-phase Reynolds number of 28329. These values (DR) obtained by polymer mixtures were higher than the DR obtained by individual polymer alone at the same conditions. An increase in βo decreased DR due to decrease in the Reynolds number of the water phase. The rigidity and interaction between the polymer mixtures molecules may be responsible for the synergism in DR. The result showed that DR effectiveness can be improved by combining high molecular weight artificial and natural drag reducing polymers.

Keywords: Drag reduction, synergism, polymers, polymer mixture, Oil-water flow.

INTRODUCTION

Transporting crude oil in pipeline systems is usually in mixture with water (1). High amount of pumping energy is required to overcome the pressure drop buildup in pipeline flow of these two immiscible fluids. The maintenance and installation of these pumps can lead to high operational cost in process industry. Hence, one of the key operations in oil and gas industry is the pipelines transportation of fluids (1-3).

Many researchers have proved that frictional pressure loses in pipeline flows can be reduced by adding small amount of higher molecular weight polymeric solution which is referred to as drag reduction (DR) (3-4). Thus, the pumping energy

requirement is reduced (5-6). DR has many industrial applications in different field which include drilling of oil from reservoir, crude oil pipeline transportation, filtration, irrigation and extraction among others (1, 7, 8). Recently, it was suggested for transportation of drinking water due to its harmless properties (9).

Drag reducing polymers (DRPs) are divided into artificial drag reducing polymer (HPAM, PEO, among others) and natural drag reducing polymer (guar gum, AVM, carboxymethyl cellulose among others). The efficiency of the natural drag reducing polymers is less than that of HPAM and PEO due to their rigidity but are more environmentally friendly (10-13). The incorporation of natural drag reducing polymer (AVM) onto HPAM and PEO can improve

the efficacy of DR and reduce environmental impact (12-13).

However, several oil-water flow (multiphase flow) patterns have been identified and classified by researchers. These include stratified flow, stratified flow with mixing at the interface, annular flow, dispersed flow, slug flow and plug flow among others (6-7). Multiphase flow patterns depend on density, viscosity, velocity, inclination and diameter, pipe roughness, surface wetting, and interfacial tension (14). Also, in multiphase flow Re is a function of density, viscosity, pipe diameter, superficial or mixture velocity, temperature, pressure and each phase volume fraction (14-15). The present research is limited to the use of polymer mixtures (HPAM+AVM and PEO+AVM) on pressure drop in pipeline multiphase flow (MPF). DR on oil-water flow have been carried out by many researchers (14-20).

Abubakar et al. (14) also studied DR with co-polymer (AN 105-SH) in horizontal oil-water flows in relatively large pipe diameter of 74.7 mm ID and length of 12 m. They reported that DR increased with increase in mixture velocity but decreased with increase in oil input volume fraction (βo). Edomwonyi-Otu and Angeli (1) explored on the effect of polymer addition on pressure drop and interfacial waves in horizontal oil-water flows using HPAM in 14 mm ID acrylic pipe with middle distillate as oily phase. They reported that mixture velocity affected the pressure drop in oil-water flows and small amount of DRP reduces drag for both single and multiphase flow. Al-Wahaibi et al. (16) studied effect of pipe diameter (19 mm and 25.4 mm) on DR in horizontal oil-water flows using magnafloc 1035 with concentration ranging from 2 – 30 ppm. DR of 60% in 25.4 mm and 45% in 19 mm ID pipe was achieved. Langsholt (17) used both water and oil soluble polymers at mixture velocity of 1.5 m/s. It was reported that DR in oil-water flows increased with increase in βo of the drag reducing polymer soluble phase. Yusuf et al. (6) studied the effect of drag reducing polymer on pressure drop using Magnafloc 1035 with concentration ranging from 2 - 10 ppm in a horizontal pipe diameter of 25.4 mm ID and length of 8 m using high viscous oil (mineral oil). A maximum DR of 60% was achieved. Omer and Pal (18) also used two different molecular weight PEO and carboxymethyl cellulose with concentration ranging from 0 -1 wt% each, in different horizontal pipe ID. They observed a negative effect on pressure drop due to the insolubility of the drag reducing polymers in the oil phase. Al-Yaari et al. (19) used three different molecular weights of PEO of concentrations ranging from 10-15 ppm in 25.5 mm ID horizontal pipe and using kerosene as the oil phase. They reported that pressure drop is a function of water fraction, mixture velocity,

concentration and molecular weight of the drag reducing polymer and drag DR efficiency (DRE) decreases in the presences of salt water. Though, Al-Wahaibi et al. (20) was the first to report a documented work on DR in oil-water flows. They investigated the effect of two concentrations (20 & 50 ppm) of Magnafloc 1011 in 14 mm ID horizontal acrylic pipe on oil-water flows. They achieved the maximum DR of 50%. They also observed that pressure drop decreases with increased in the water phase velocity which is similar with the findings of Al-Yaari et al. (19).

Despite the works done in understanding the mechanism of DR in oil-water flow using polymer mixtures, the literature is rather insufficient. There is also the need to develop robust models for the accurate prediction of DR in synergistic system and these require a lot of data than is currently available. Thus, the main focus of this work is to study the effect of the combine polymer mixtures (HPAM+AVM and PEO+AVM) in horizontal oil-water flows.

METHODS

Description of the flow facility
The diagrammatic representation of the flow facility is shown in Figure 1. It is divided into three main parts: the handling section, pumping or regulating section and the flow measuring section. The handling section consists of three tanks where the fluids are stored: the oil, and water tanks are each 200 litres while the separator is 220 litres in capacity. Gravity is the main principle of separation in the separator where water is drained through the bottom opening while the separated oil is recycled. The 20 mm ID unplasticised polyvinylchloride (uPVC) pipes are each connected to water and oil tanks and m. The centrifugal pumps (model Jet 102M/N.31227) with maximum flow rate of 65 L/min each were used to circulate the test fluids into the test section. The flow rates which were measured with variable area flow meters (LZM-20J; ±3% accuracy) are controlled by gate valves and are separated for each fluid. The meter for the water line flows at ≤ 24 GPM or 100 LPM and it was calibrated before the experiments begin. The injection port for the polymer master solution is located by the side of the water pipeline before the Y-junction. The programmable peristaltic injection pump (model NE-9000; ±1% accuracy) was used to add the master solution in the water line. The internal diameter of the acrylic pipe is 20 mm ID with a length greater than 140*D from the mixing point (Y-junction) to the next pressure measuring point, which are 1.5 mm in size at lower portion of the pipe walls. They were at a location that ensures that fully developed flow in the test section is attained before measurements.
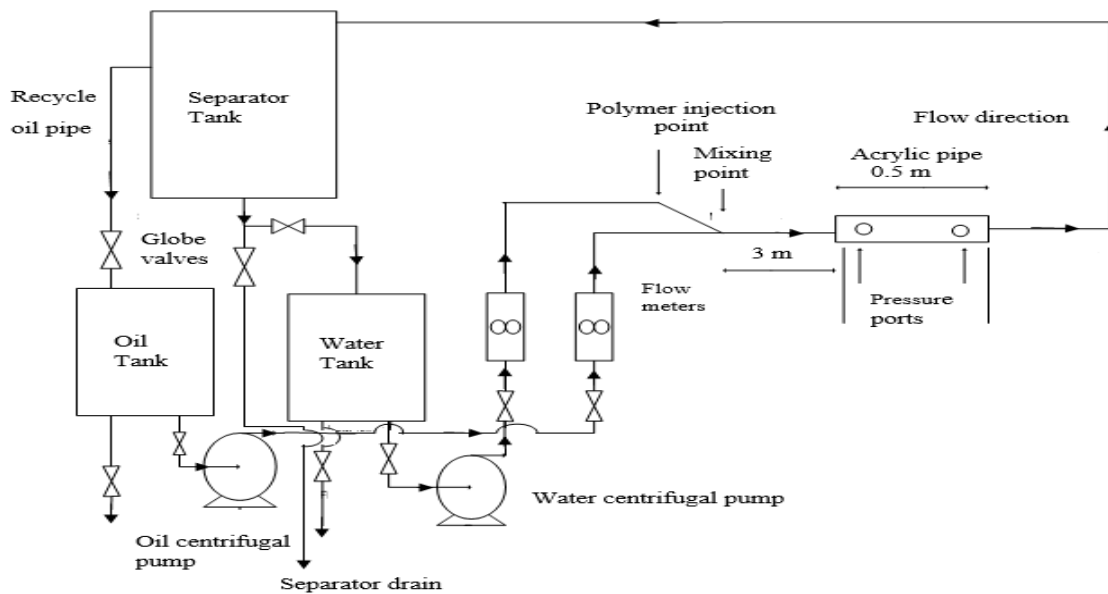
Figure 1: Schematics of experimental flow rig.

Polymer preparation

The polymers used are partially hydrolysed polyacrylamide, HPAM (Magnafloc 1011) manufacture by BASF chemicals 10×10^6 g/mol, polyethylene oxide (PEO) manufacture by Sigma-Aldrich with average molecular weight of 8×10^6 g/mol, and Aloe Vera mucilage (AVM) extracted from Aloe Vera plant. All the polymers are water soluble and were used without further purification. The individual solutions of the polymers were prepared firstly, before the solution of polymer mixture. A master solution of 2000 ppm of each of the synthetic polymer was prepared as follows. 10 g of each of the polymeric powder was measured using weighing balance (Kerro, BLC 3002) and gently spread over 5 litres of surface of water and stirred for 3 hours with a mechanical stirrer (Gilverson, L28) at a very low speed (to avoid degradation of the polymer) for the mixture to be completely homogenised. The stirred solution was left for 12 hours, mostly overnight, to ensure complete dissolution of the polymeric particles and removal of trapped gas bubbles to form the master solution (21, 7). Aloe Vera leaves were harvested from a garden then washed thoroughly. The leaves were then cut vertically on both sides and soaked in water for 10 minutes, to remove the Aloin within them. The leaves were then peeled and the Aloe Vera mucilage (AVM) was extracted by scraping and sieving the gel from the leaves (22). Aloe Vera leaf contains about 98% water while the remaining 2 % is the AVM (23-24). 20,000 ppm master solution of AVM was prepared. AVM suffers biological degradation in 24 hours. After the preliminary experiments with each of the polymer solutions in single phase water flow, the total concentration (tc) for any mixture was chosen based on the fact that at least one of the polymers in the mixture gave maximum DR at that concentration (25). In case of this work, 30 ppm

and 400 ppm were selected as the total concentration for the mixture of HPAM-AVM and PEO-AVM. The mixtures master solution of 2000 ppm and 20,000 ppm were prepared at different mixing ratio to achieve the required concentration of the polymer mixtures in the flow line as described by Reddy & Singh and Malhotra et al. (26, 25). 200 millilitres of 20,000 ppm of AVM master solution was measured and diluted with 8000 millilitres of water to achieved 500 ppm. 1500 ppm of the synthetic polymers (HPAM & PEO) was mixed with 500 ppm of AVM and stirred for 3 hours and the stirred solution was left for 12 hours to form a master solution of 2000 ppm for the polymer mixtures. It was injected into the aqueous phase at specific flow rate in order to achieved the require concentration in the water flow line.

Procedure

The injection pump and flow metres were tested before running the experiments to ensure accurate delivery of the required amounts of oil and water into the test section, and the polymeric master solution into the water phase. The experiment was carried out in horizontal pipe diameter of 20 mm ID and length of 140*D at ambient conditions (25 °C, 1 atm). The U-tube manometer was used to for the pressure drop measurement. The experiments were performed at least three times with a standard deviation less than 2.5%. HPAM, PEO, AVM, HPAM+AVM and PEO+AVM were tested at different concentrations and Reynolds numbers. The concentrations of HPAM and PEO ranging from 2.5 - 100 ppm while the concentration of Aloe Vera mucilage (AVM) ranging from 5 - 500 ppm at flow rates of 10 L/min, 20 L/min, 30 L/min and 40 L/min (Re from 12916 - 48871). The optimal polymer concentration of 30 ppm (for HPAM & PEO) and 400 ppm (for AVM) were obtained from preliminary experiments of a single-phase water flow. The

optimal concentrations were selected to be the total concentration (tc) for the polymer mixture (25). The preliminary experiment of the polymer mixtures (HPAM+AVM & PEO+AVM) was conducted at different mixing ratio for the tc of 30 ppm and 400 ppm at different Re (12916 - 48871). The mixing ratio of 3:1 and 1:19 was chosen due the fact that, maximum DR was achieved at that mixing proportion from the preliminary experiment conducted. HPAM, PEO, AVM, HPAM+AVM and PEO+AVM were tested at different oil input volume fraction (β_o) and mixture Reynolds number (Mix-Re; mixture velocity, Umix). The Mix-Re was obtained from the summation of the water phase Reynolds number and that of the oil phase, at different superficial velocities of water (Usw) and oil (Uso). The concentrations of 30 ppm (HAPM & PEO) and 400 ppm (AVM) were tested at Reynolds number of 37773. The various proportion of the oil input volume fractions were 0, 25, 50, 75 and 100%.

The pressure drop was recorded and used for calculation of DR; defined by the given Equation 1 below:

$$DR = \frac{\Delta P_W - \Delta P_\wp}{\Delta P_W} \times 100\%$$

Where; ΔP_W and $\Delta P_\wp$ is pressure drop of the fluid with and without DRPs.

RESULTS AND DISCUSSION

Only the mean values of the pressure drop obtained from three measurements were used in the calculation of percentage drag reduction (DR). The DR calculated using Equation 1 was presented graphically in two ways; at first DR against βo at different Mix-Re and second against Mix-Re at different βo.

DR in Single Phase Water Flow
The DR of HPAM, PEO, AVM, HPAM+AVM & PEO+AVM was studied in single phase water flow at

different concentrations and Reynolds number. The maximum DR of 50%, 70% & 72%, for AVM, HPAM & PEO; 75.2% & 82.5% for HPAM+AVM (3:1 & 1:19) and 78% & 83% for PEO+AVM (3:1 & 1:19) respectively were obtained. The optimal concentration of 30 ppm (HPAM & PEO), 400 ppm (AVM), 22.5 ppm – 7.5 ppm (HPAM+AVM & PEO+AVM at tc of 30 ppm), and 20 ppm – 380 ppm (HPAM+AVM & PEO+AVM at tc of 400 ppm) were achieved at Reynolds number of 37773 in the preliminary experiments. The results obtained are in agreement with the work of Reddy & Singh (25) and Malhotra et al. (26).

DR by Polymers in Multiphase flow
The DR of HPAM, PEO and AVM was studied in MPF at different βo and Mix-Re. Figures 2 - 4 show the results of the effect of βo and Mix-Re on DR in oil-water flows for HPAM, PEO and AVM. It was observed that DR declined with increase in βo due to decrease in the Reynolds number of the water dominated region because the drag reducing polymers (HPAM, PEO and AVM)) used were only soluble in the water phase. This agree with the findings of Yusuf et al. (6) and Edomwonyi-Otu et al. (7).

Moreover, At 75 -100% βo, high pressure drop was observed owing to the fact that the larger portion of the pipe was occupied by the oily phase, which reduces the Reynolds number of the water phase, as such reduced the DR. It was also observed that increased in Mix-Re increases Usw, which creates high degree of turbulence in the water phase thus cause better interaction between the DRPs and turbulent eddies. At high turbulence in the water phase DRPs suppress the formation and propagation of this eddies which reduce the pressure drop as well the pumping energy in oil-water flow. This corroborate with the previous findings of (6-7, 14-16, 20-21).

DR of 61.67%, 58.33% and 43.33% for PEO, HPAM and AVM respectively were achieved at 25% βo and water phase Reynolds number of 28329.
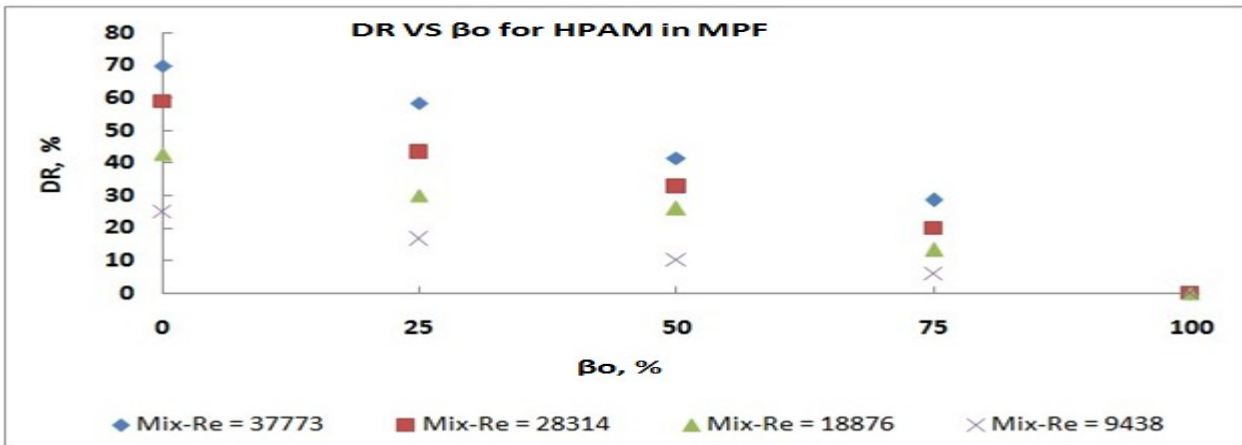
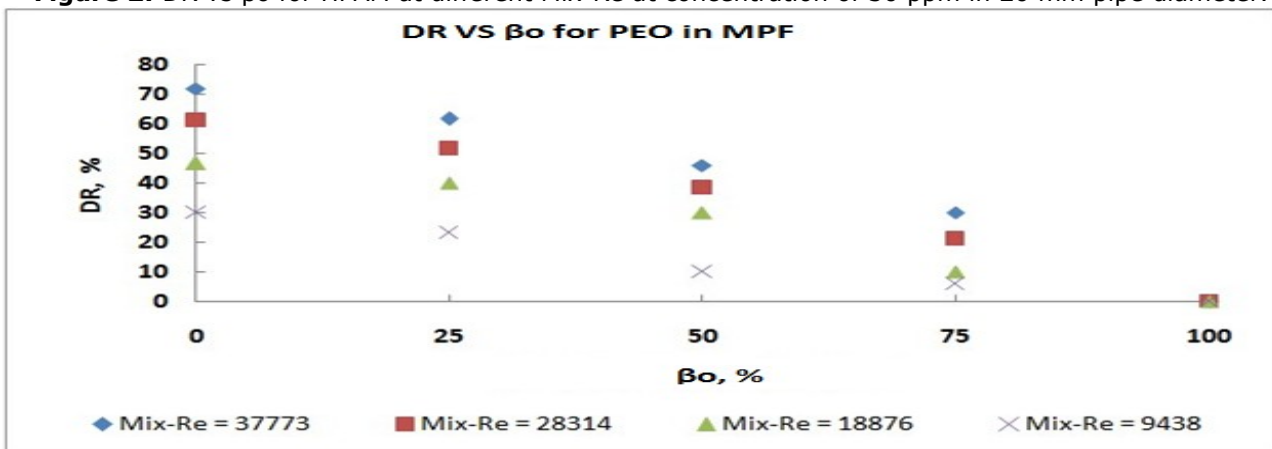**Figure 2:** DR vs βo for HPAM at different Mix-Re at concentration of 30 ppm in 20 mm pipe diameter.

Figure 3: DR vs βo for PEO at different Mix-Re at concentration of 30 ppm in 20 mm pipe diameter.
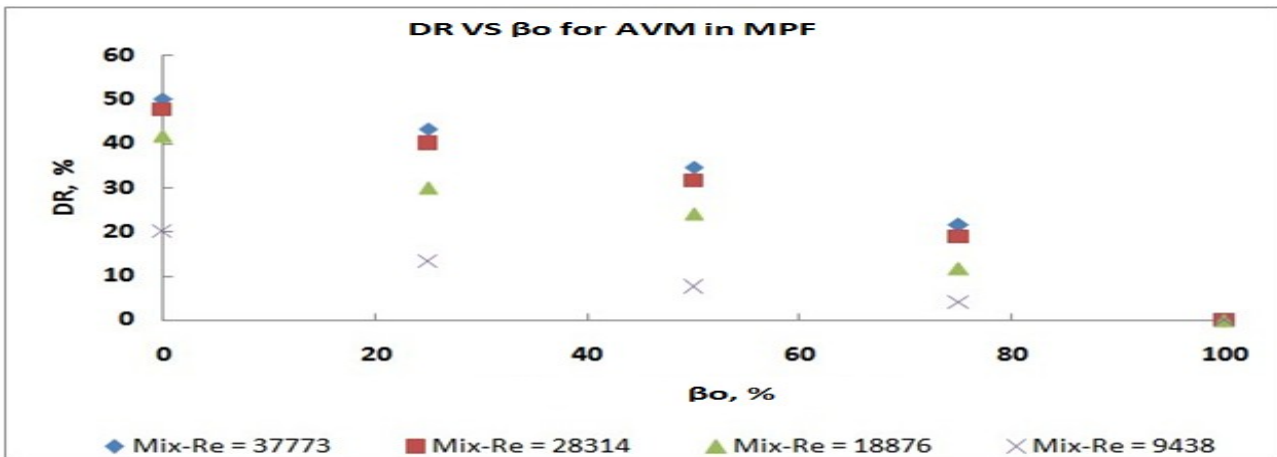

Figure 4: DR vs βo for AVM at different Mix-Re at concentration of 30 ppm in 20 mm pipe diameter.

DR Polymer Mixtures in Multiphase Flow

The DR of HPAM+AVM and PEO+AVM was studied in oil-water flows at different βo and Mix-Re. The total concentration (tc) of 30 ppm and 400 ppm at mixing ratio of 3:1 and 1:19 for the master solution of 2000 ppm and 20,000 ppm were used for the polymer mixtures. Figures 5 - 8 show the results of the effect of βo and Mix-Re on DR in oil-water flows for a mixture of HPAM+AVM and PEO+AVM. Similar declination in DR observed resulted from decrease in water phase Reynolds number due to decrease in Mix-Re (27-28). It was also observed that at the same conditions DR obtained by the polymer mixtures (61.67% & 66.67% for HPAM+AVM at 3:1 & 1:19; 63.33% & 68.33% for PEO+AVM at 3:1 & 1:19) was higher than the DR of each polymer present in the polymer mixture. The synergy in DR in the oil-water flow by polymer mixtures may be

due to the presence of other polymer molecules which improve the rigidity (flexibility) of the DRPs (27-28)(29, 25).

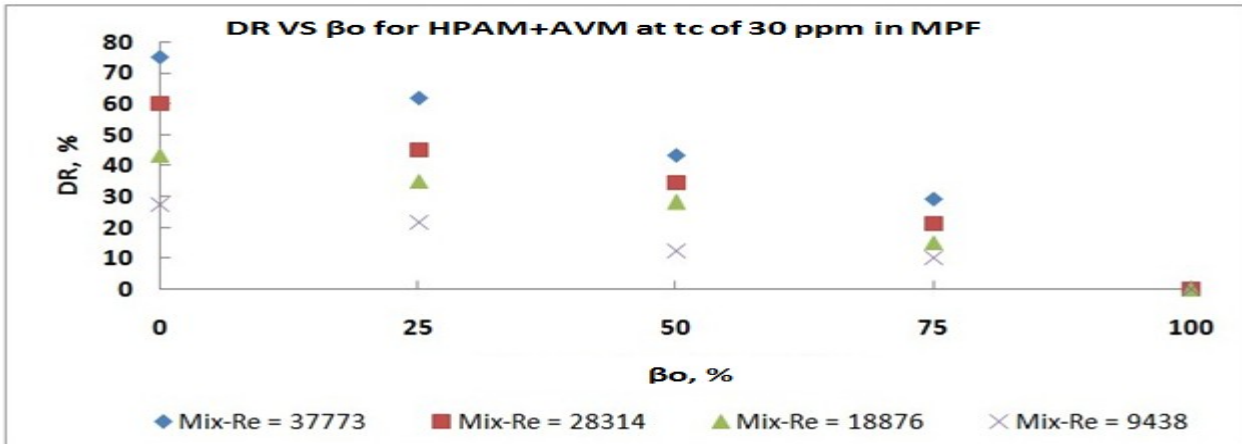used, this is in agreement with the previous works (29, 25).

Figure 5: DR vs βo for HPAM+AVM mixture ratio of 3:1 at different Mix-Re and tc of 30 ppm in 20 mm pipe diameter.
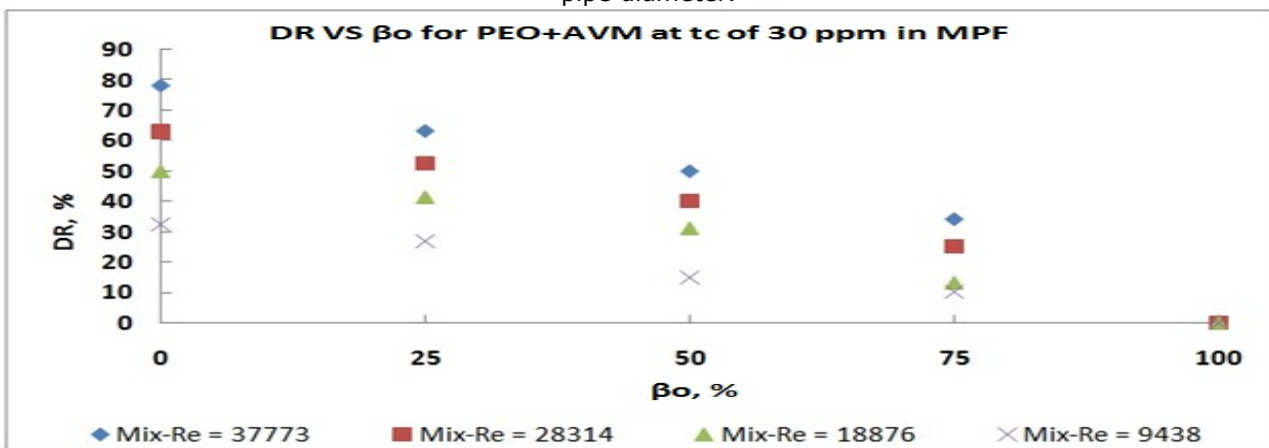

Figure 6: DR vs βo for PEO+AVM mixture ratio of 3:1 at different Mix-Re and tc of 30 ppm in 20 mm pipe diameter.
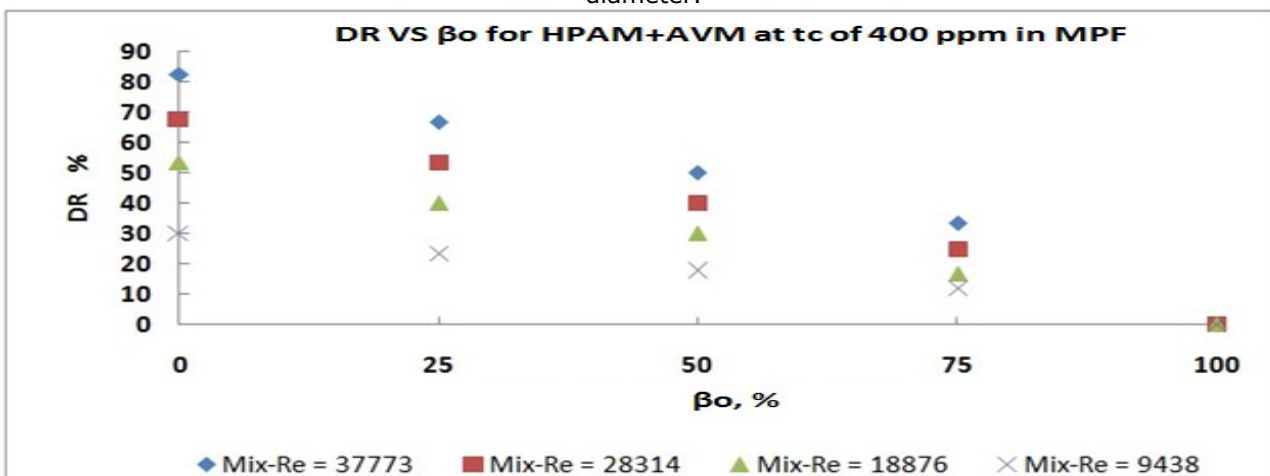

Figure 7: DR vs βo for HPAM+AVM mixture ratio of 1:19 at different Mix-Re and tc of 400 ppm in 20 mm pipe diameter.
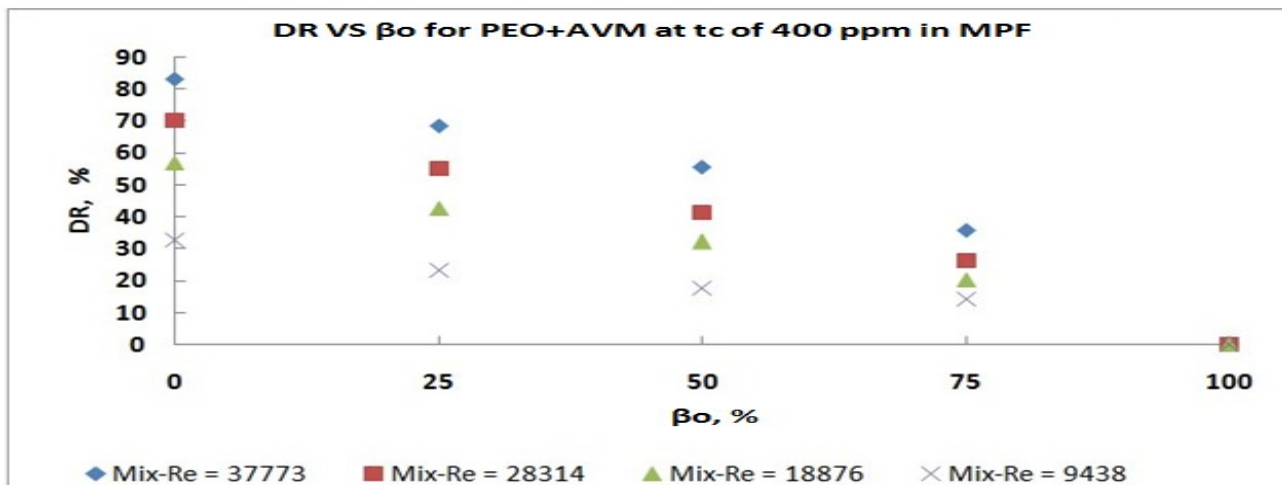
Figure 8: DR vs βo for PEO+AVM mixture ratio of 1:19 at different Mix-Re and tc of 400 ppm in 20 mm pipe diameter.

REFERENCES

X1. Edomwonyi-Otu LC & Angeli P. Effects of Polymer Addition on Pressure Drop and Interfacial Waves in Horizontal Oil-Water Flows. Petroleum Technology Development Journal. 2014 July; (2): 41–8.

2. Al-Sarkhi A. Drag reduction with polymers in gas–liquid/liquid–liquid flows in pipes: a literature review. Journal of Natural Gas Science and Engineering. 2010; 2: 41–8.

3. Gyr A & Bewersdorff HW. Drag reduction of turbulent flows by additives. Fluid Mechanics and Its Applications. 1995. 32, xi, p 234.

4. Ting RY & Little RC. Characterization of drag reduction and degradation effects in the turbulent pipe flow of dilute polymer solutions. Journal of Applied Polymer Science. 1973; 17(11): 3345–56.

5. Virk PS, Merrill EW, Mickley HS, Smith KA, & Mollo-Christensen EL. The Toms phenomenon: turbulent pipe flow of dilute polymer solutions. Journal of Fluid Mechanics. 1967; 30(2): 305–28.

6. Yusuf N, Al-Wahaibi T, Al-Wahaibi Y, Al-Ajmi A, Al-Hahmi AR, Olawale AS. Mohammed IA. Experimental study on the effect of drag reducing polymer on flow patterns and drag reduction in a horizontal oil–water flow. International Journal of Heat and Fluid Flow. 2012; 37: 74–80.

7. Edomwonyi-Otu LC, Chinaud M & Angeli P. Effect of drag reducing polymer on horizontal liquid-liquid flows. Experimental Tharmal and Fluid Science. 2015; 64: 164 -74.

8. Marmy RMS, Hayder AB & Rosli MY. Improving the flow in pipelines by Cocos nucifera fiber waste. International Journal of Physical Science. 2012; 7(26): 4073–80.

9. Edomwonyi-Otu LC, Simeoni M, Angeli P & Campolo M. Synergistic Effect Of Drag Reducing Agents In Pipes Of Different Diameters. Nigerian Journal Of Engieering. 2016; 22: 1- 5.

10. Deshmukh SR & Singh RP. Drag reduction characteristics of graft copolymers of xanthan gum and polyacrylamide. Journal of Applied Polymer Science. 1986; 32: 6163–76.

11. Edomwonyi-Otu LC & Adelakun DO. Effect of Heavy Molecular Weight Polymer on Quality of Drinking Water. Materials Today Communications. Elsevier Publication. 2018; 15: 337-43.

12. Nour AH, Nuraffini K & Hayder AS. Grafted Natural Polymer as New Drag Reducing Agent : An Experemental Approach. Chemical Industry and Chemical Engineering Quarterly. 2012; 18(3): 361–71.

13. Singh RP. Advanced Turbulent Drag Reducing and Flocculating Materials Based on Polysaccharides. Polymers and Other Advanced Materials. 1995; 75: 227–49.

14. Abubakar A, Al-Wahaibi T, Al-Wahaibi Y, Al-hashmi AR & Al-Ajmi A. Drag reduction with polymer in oil-water flow in relatively large pipe diameter. International Journal of Advanced and Applied Science. 2016; 2(12): 1–6.

15. Eshrati M, Al-Hashmi AR, Al-Wahaibi T, Al-Wahaibi Y, Al-Ajmi A, & Abubakar A. Drag reduction using high molecular weight polyacrylamides during multiphase flow of oil and water: A parametric study. Journal of Petroleum Science and Engineering. 2015; 135: 403–9.

16. Al-Wahaibi T, Al-Wahaibi Y, Al-Ajmi A, Yusuf N, Al-Hashmi AR, Olawale AS & Mohammed IA. Experimental investigation on the performance of drag reducing polymers through two pipe diameters in horizontal oil-water flows. Experimental Thermal and Fluid Science. 2013; 50: 139–46.

17. Langsholt M. An Experimental Study on Polymeric Type DRA used in Single- and Multiphase Flow with Emphasis on Degradation, Diameter Scaling and the Effects in Three-phase Oil–Water–Gas Flow. Institute for Energy Technology (IFE), Norway, 2012.

18. Omer A, Pal R. Pipeline flow behavior of water-in-oil emulsions with and without a polymeric additive. Chemical Engineering Technology. 2010; 33(6): 983–92.

19. Al-Yaari M, Soleimani A, Abu-Sharkh B, Al-Mubaiyedh U & Al-Sarkhi A. Effect of drag reducing polymers on oil–water flow in a horizontal pipe. International Journal of Multiphase Flow. 2009; 35: 516–24.

20. Al-Wahaibi T, Smith M & Angeli P. Effect of drag-reducing polymers on horizontal oil-water flows. Journal of Petroleum Science and Engineering. 2007; 57(3-4): 334–46.

21. Abubakar A, Al-Wahaibi T, Al-Wahaibi Y, Al-Hashmi AR & Al-Ajmi A. Roles of drag reducing polymers in single- and multi-phase flows. Chemical Engineering Research and Design. 2014; 92(11): 1–29.

22. Bari HAA, Letchmanan K & Mohd YR. Drag Reduction Characteristics Using Aloe Vera Natural Mucilage: An Experimental Study. Journal of Applied Science. 2011; 11(6): 1039–43.

23. Bozzi A, Perrin C, Austin S. Quality and Authenticity of Commercial Aloe Vera Gel Power. Food Chemistry. 2007; 103: 22-30.

24. Davis R.H. Aloe Vera-A Scientific, Approach. Vantage Press Inc., New-York, USA, 1997; p. 290-306.

25. Reddy GV & Singh RP. Drag reduction effectiveness and shear stability of polymer-polymer and polymer-fibre mixtures in recirculatory turbulent flow of water. Rheologica Acta. 1985; 24: 296–311.

26. Malhotra JP, Chaturvedi PN, & Singh RP. Drag Reduction by Polymer-Polymer Mixtures. Journal of Applied Polymer Science. 1988; 36: 837–58.

27. Abubakar A, Al-Hashmi AR, Al-Wahaibi T, Al-Wahaibi Y., Al-Ajmi A, & Eshrati M. Performance of a drag-reducing polymer in horizontal and downward-inclined oil-water flow. Chemical Engineering Research and Design. 2015; 104: 1–28.

28. Yusuf N, Olawale AS & Mohammed IA. Chemical Engineering Research and Design Effect of oil viscosity on the flow structure and pressure gradient in horizontal oil – water flow. Chemical Engineering Research and Design. 2011; 90(8): 1019–30.

29. Dingilian G & Ruckenstein E. Positive and Negative Deviations from Additivity in Drag Reduction of Binary Dilute Polymer Solutions. AlChE Journal. 1974; 20(6): 1222–4.

The Effect of Different Drying Methods-Temperatures on Drying Time and Vitamin C in Pineapple, Kiwi, and Avocado Fruits

Ayşe BİÇER ✉ **, Filiz KAR*** ✉ iD

Fırat University, Engineering Faculty, Department of Chemical Engineering, Elazığ, Turkey.

Abstract: In this study, kiwi, pineapple, and avocado fruits were dried at different temperatures and different types of dryers and Vitamin C detection was performed prior to and after drying. In order to determine the impact of the geometric shape of the fruit on drying, drying experiments were performed using fruits cut in cubic (1x1x1 cm), rectangular prism (1×1×2.5 cm) and spherical (1 cm diameter) shapes. The drying behaviors of 3 different fruits have been observed in tray dryer setting at 1.5 m/s air velocity, 45 °C and 55 °C temperature and infrared dryer. An examination of the data obtained at the end of the drying procedures yielded that, at 55°C drying temperature, drying occurred without any change in the color of samples. In the experiments made for pineapple, it has been observed that drying took an average of 420 minutes, that the velocity of moisture loss was highest with cubic shape, followed by rectangular and spherical shapes; as for the experiments made with kiwi, it has been observed that drying took 360 minutes on average and the velocity of moisture loss was highest with cubic shape, followed by rectangular and spherical shapes. About avocado fruit, the drying took 400 minutes on average and its geometric behavior is similar to the other fruits. The effective parameter for the drying of fruits in both flat flow and infrared is temperature. The drying periods of pineapple, kiwi, and avocado in infrared dryer are 400, 240, and 390 minutes, respectively. Among the examined fruits, pineapple and kiwi are rich in Vitamin C (before drying). At the end of the conducted experiments, ascorbic acid amount has been found as 485, 1002, and 75 mg/kg, respectively. After the drying procedure, vitamin C values were detected as 187, 25.9 and 385.4 mg/kg. These results show that 60-65% of vitamin C is lost during drying procedure. Page, Henderson & Pabis, and Logarithmic thin layer drying models, available in the literature were used to evaluate the experimental data. All the models were compared according to statistical parameters; i.e. model efficiency (R^2), chi-square (χ^2) and root mean square error (RMSE). It was observed that Modified Page model among the models used is best mathematical model represented the drying behavior of tropical fruits.

INTRODUCTION

Food materials can be spoiled by individual or combined effects of physical, biological, or chemical factors. Microorganisms (bacteria, mould, yeast), enzyme activities, lipid oxidation (oxidative rancidity), non-enzymatic browning (Maillard) events and physical impacts (striking, heat, etc.) can lead to such spoilage. In order to prevent the physical, biological or chemical factors that lead to spoilage, a variety of food preservation methods are being used. These include such methods as drying, thermal process (pasteurization/sterilization), fermentation, adding preservative materials (salting and sugaring), fuming (smoking), canning, freezing, cold-preserving and irradiation (1,2).

Drying is a process which occurs in nature spontaneously. People have observed nature and discovered that sun drying can protect

foods. So they started to dry agricultural products. Today drying can be done industrially and more rapidly and healthily due to the increase in mechanization (3-6). Drying is reducing the water activity (aw) under a value preferred for food and making it durable against microbiological, chemical and enzymatic spoilage (7-9). The purpose of drying food materials is to prevent the spoilage of food, preserving its nutrient value and quality features, reducing its dimension for transportation and storage, and removing maximum amount of water in the food using minimum energy. Choosing the most suitable drying method in terms of energy consumption and economy is essential (10).

The drying process in the presence of surrounding hot air could be considered as one of the viable option to accomplish the satisfactory evaporation of moisture from fruits. The drying process could be defined as a progress of removal of moisture via simultaneous heat and mass transfer between the sample and the surrounding atmosphere by means of vaporization, generally caused by temperature and air convection forces (11).

The aim of this study is to dry kiwi, pineapple, and avocado fruits with two different methods in different geometric shapes and to determine the vitamin C values before and after drying. In addition, drying data were applied to various models and the most appropriate model was determined by statistical analysis.

MATERIAL AND METHOD

Information on the fruits used in experiments
Pineapples (*A. comosus var. Perola*), kiwi (*Actinidia deliciosa)* and avocado (*Persea americana*) were purchased in a local market in Elazığ, Turkey. Fruits were washed and peeled. The fruits were cut in appropriate geometric shapes and used in experiments.

Kiwi is the common name given to the plants in cultivar group obtained from *Actinidia deliciosa,* which is a grapevine-like arboreal climbing plant, and the hybrids of *A. deliciosa* and other *Actinidia* species; it is also used for the edible fruits of these plants.

In recent years kiwi fruit has been begun to be farmed in and around Artvin, Yalova, Adapazarı, Rize, Ordu and Antalya/Turkey. Kiwi includes high levels of potassium, fiber, and vitamins A, E and C and potassium, kiwi is also rich in calcium, iron, and magnesium minerals. Kiwi has a high nutritive value and

even one kiwi can meet the entire daily need for Vitamins A and C (12).

Pineapple (*Ananas comosus*) is a plant from Bromeliaceae family, which grows in warm countries; the word is also used to refer to the fruit of that plant. Its home is South America. Its fruit is big, fragrant and delicious, and it has a bunch of leaves on top (13, 14).

Avocado (Persea Americana) is a tree belonging to the Lauraceae family, which also includes cinnamon and camphor tree which is in the class Angiospermae (division Magnoliophyta), whose homeland is the central part of Mexico; this word is also used to denote the fruit of this tree. Its plant is cultivated in all warm climates; in Turkey, it is planted between Antalya and İskenderun in Mediterranean region and in eastern Black Sea region provinces such as Rize where frost is rare. On the back of rapidly growing global demand, world production of avocado reached an estimated 6.3 million tonnes in 2018, representing a 6.7 percent increase from 2017. Among all the major tropical fruits, avocado has seen the fastest production growth in the last decade, at an annual average rate of 6 percent, primarily due to increases in harvested area in the major producers (15). The consistent rise in the agriculture of avocado fruit is attributed to its increasing requirement as a consequence of numerous benefits of the same on human health (16,17). There have been many studies on avocado (18-20).

Straight air-flow experiments in tray dryer
Prior to beginning the experiments, dryers were operated idly for 30 minutes and the regime conditions were created as regards the internal temperatures of dryer rooms. The experiments were repeated in tray dryers for the straight flow condition of heating air at 1.5 m/s air velocity and 45 ^{o}C, 55 ^{o}C air temperatures (Figures 1-2). In the second experiment mechanism, the infrared dryer was operated at 55 ^{o}C temperature (Mettler LJ16).

The straight air flow tunnel-type dryer blower used in experiments includes electrical heater, thermometers, dryer trays, and precision scales. Drying air was heated through electrical resistance wires which were placed at the outlet of the blower and air temperature was adjusted using temperature control knob. Air velocity was controlled using a speedometer held at the air outlet through speedometer knob.
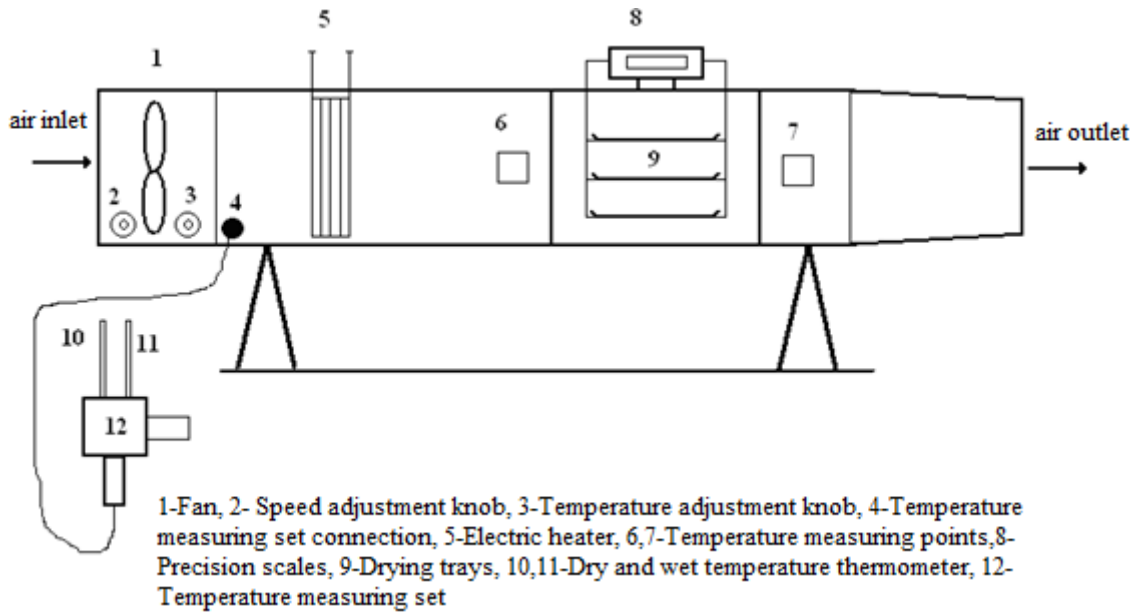
1-Fan, 2- Speed adjustment knob, 3-Temperature adjustment knob, 4-Temperature measuring set connection, 5-Electric heater, 6,7-Temperature measuring points,8-Precision scales, 9-Drying trays, 10,11-Dry and wet temperature thermometer, 12-Temperature measuring set

Figure 1. Tray type dryer (21)

Figure 2. Fruits in tray dryer.

Ascorbic acid (vitamin C) content of dried fruits

Using HPLC device, the ascorbic acid standard curve required for ascorbic acid designation was determined and data were evaluated using this curve (22).

Calculations made to determine drying characteristics and Drying Model Equations

During the drying of fruits samples in cabin-type dryer moisture content is calculated as follows:

$$M_t = \frac{(m-KM)}{KM} \qquad (1)$$

Drying speed is found by taking the derivative of the drying time curves as per moisture content.

$$\text{Drying speed} = \frac{(M_{t+dt}-M_t)}{dt}$$
$$\text{(g water/g dry material. min.)} \qquad (2)$$

Moisture ratio is calculated as follows:
$$MR = \frac{(M_t-M_e)}{(M_o-M_e)} \qquad (3)$$

While drying food materials with hot air, M_e value is negligible compared to M_t and M_o. For this reason, it is reported that Me value could be taken as zero in the calculations (23).

While using MR values M_t/M_o equation was used directly.

Previous studies include equations which are used to design drying processes, ensuring large-scale drying and improving drying processes. Among these equations, experimental drying data can be used to determine the model which best represents drying (24-29).

The constants in models were determined by the non-linear regression analysis to examine the goodness-of-fit of the models. Statistical software package (Statistica for Windows 5.0, 1995) was used to perform the nonlinear regression analysis of experimental drying data. The quality of the fit of the model was estimated using the various statistical parameters such as root mean square error (RMSE), chi-square (χ^2), mean bias error (MBE), mean percentage error (MPE) and the coefficient of determination r^2 (30).

Determination of diffusion coefficient
Diffusion, which occurs during the drying of food materials, is a complicated process. In decreased speed period, the drying parameters of biological products can be defined using Fick's diffusion equation

(31,32). Diffusion coefficient is an important parameter in drying, and was calculated using different velocities and temperatures for fruits. For sliced fruits for which diffusion coefficient is fixed and the first moisture content is homogeneous, this equation was obtained by Crank as follows (33).

$$MR= \frac{M-M_e}{M_i-M_e} = \frac{8}{\pi}\sum_{n=0}^{\infty} \frac{1}{(2n+1)^2} \exp\left(\frac{-(2n+1)^2\pi^2 D_{eff}t}{4L^2}\right) \ (4)$$

where D_{eff} is diffusion coefficient (m²/s), L is the semi-thickness of dried products, and t is drying period. This equation can be simplified as based on the first term of series for long drying processes (34).

$$MR= \frac{M-M_e}{M_i-M_e} = \frac{8}{\pi}\sum_{n=0}^{\infty}\left(\frac{-\pi^2 D_{eff}t}{4L^2}\right) \ (5)$$

Diffusion coefficient can be found by solving Equation (5) using regression analysis.

EXPERIMENTAL RESULTS

Geometric shapes of the samples were chosen as cubic (1×1×1 cm), rectangular prismatic (1×1×2.5 cm) and spherical (1 cm diameter) which were placed separately into the dryers (Figure 3).

Figure 3. Dried fruits.

Experiments performed at tray dryer
As a result of the experiments conducted in tray dryer at 45 an 55 °C, it was found out that drying was faster at 55 °C. For this reason, effort was paid to determine how geometric shape of the material would affect drying at fixed temperature and air velocity.

The results of fresh food drying processes conducted for tray dryer are given in Figure 4. As a result of the examination of Figure 4, it was observed that at 1.5 m/s drying velocity and 55°C drying temperature the color of the samples did not change, which meant that drying was realized in 420 minutes without

carbonization at material level. An examination of Figure 4 shows that cube is the geometric shape which witnessed fastest moisture removal followed by rectangular prism and sphere.
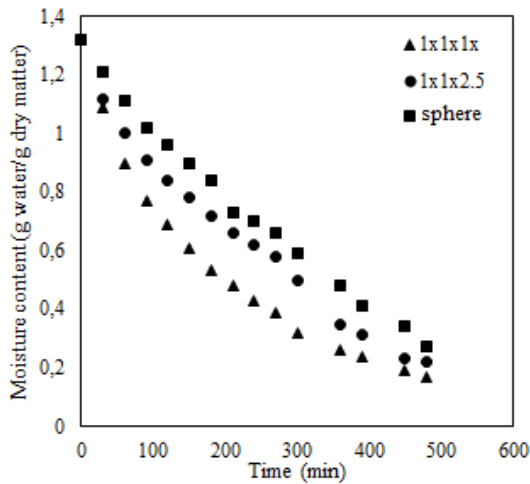
Figure 4. Variation in moisture content as a function of drying time (pineapple fruit).
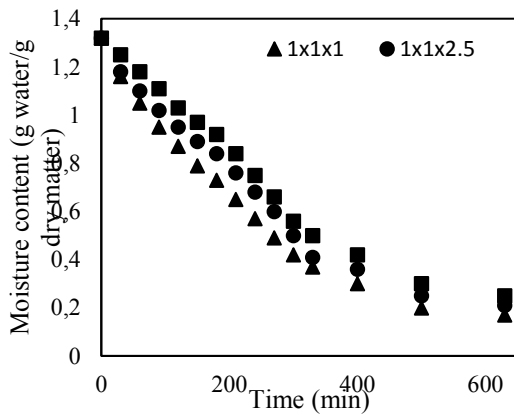

Figure 5. Variation in moisture content as a function of drying time (avocado fruit)

As for avocado fruit, it is seen that average drying took 500 minutes and, similar to the other fruits given above, drying was fastest in cubic shape followed by rectangular prismatic and spherical (Figure 5).

Figure 6. Variation in moisture content as a function of drying time (kiwi fruit)

The experiments conducted for kiwi showed that average drying period was 360 minutes and, similar to the pineapple fruit, moisture removal was fastest in cubic followed by rectangular prismatic and spherical (Figure 6).

Moisture content values were obtained by drying tropical fruits in three different geometrical shape in the tray dryer. The relevant experimental data is modeled using five different drying models and the results are presented in the Table.

Equation 5 is solved in order to determine diffusion speed. Table 1 provides the change of diffusion coefficient according to the geometric shape of fruits. An examination of the table shows that diffusion coefficient is higher in fruits sliced in 1x1x1 dimension. Results are in harmony with the data obtained in the literature (35, 36).

Table 1. Regressions for the Lewis' Model ($M_R = \exp(-kt)$).

Fruits		k	a	n	c	R²	RMSE	χ2	MBE	MPE
pineapple	1x1x1	0.0065	-	-	-	0.989	0.00047	-0.0005	0.00962	-18.8869
	1x1x2.5	0.0046	-	-	-	0.968	0.00257	-0.0027	0.02177	-102.990
	sphere	0.0049	-	-	-	0.975	0.00620	-0.0066	-0.0601	-12.7089
avocado	1x1x1	0.0054	-	-	-	0.971	0.00313	-0.0033	-0.0279	1.5188
	1x1x2.5	0.0052	-	-	-	0.928	0.00872	-0.0094	-0.0579	7.5148
	sphere	0.0035	-	-	-	0.964	0.00679	-0.0073	0.00765	-12.7089
kiwi	1x1x1	0.0091	-	-	-	0.957	0.00827	-0.0089	-0.0639	10.859
	1x1x2.5	0.0067	-	-	-	0.956	0.00433	-0.0047	-0.0335	-0.3501
	sphere	0.0057	-	-	-	0.947	0.01066	-0.0115	-0.0507	-13.3486

Table 2. Regressions for the Page model $M_R = \exp(-kt)$.

Fruits		k	a	n	c	R²	RMSE	χ2	MBE	MPE
pineapple	1x1x1	0.0062	-	1.32	-	0.987	0.00039	-0.0004	-0.0010	-14.537
	1x1x2.5	0.0059	-	1.13	-	0.985	0.00767	-0.0089	-0.0604	-36.166
	sphere	0.0055	-	1.15	-	0.990	0.00164	-0.0192	-0.0020	-11.718
avocado	1x1x1	0.0029	-	1.27	-	0.995	0.05280	-0.1616	-0.1945	56.7868
	1x1x2.5	0.0035	-	1.19	-	0.993	0.05533	-0.0645	-0.1976	50.2778
	sphere	0.0036	-	1.43	-	0.985	0.20722	-0.2417	-0.3882	77.1123
kiwi	1x1x1	0.0017	-	1.38	-	0.954	0.01727	-0.0204	-0.0985	45.1689
	1x1x2.5	0.0026	-	1.26	-	0.960	0.02200	-0.0259	-0.1169	40.5022
	sphere	0.0028	-	1.11	-	0.943	0.00559	-0. 006	-0.0119	-25.768

Table 3. Regressions for the Modified Page Model ($M_R = \exp(-kt)$).

Fruits		k	a	n	c	R²	RMSE	χ2	MBE	MPE
pineapple	1x1x1	0.2204	-	0.2813	-	0.997	0.00038	-0.0004	-0.0006	-15.8836
	1x1x2.5	0.205	-	0.274	-	0.991	0.01269	-0.0148	-0.0866	23.9696
	sphere	0.190	-	0.274	-	0.981	0.00758	-0.0088	-0.0665	8.0315
avocado	1x1x1	0.2113	-	0.3011	-	0.996	0.00658	-0.0077	-0.0557	9.6452
	1x1x2.5	0.227	-	0.2990	-	0.990	0.01795	-0.0209	-0.0995	17.8466
	sphere	0.315	-	0.3150	-	0.976	0.01694	-0.0197	-0.0927	14.2536
kiwi	1x1x1	0.2345	-	0.2703	-	0.998	0.00771	-0.0091	-0.0594	5.9008
	1x1x2.5	0.230	-	0.2540	-	0.988	0.01047	-0.0123	-0.0725	12.4995
	sphere	0.209	-	0.2980	-	0.988	0.02335	-0.0275	-0.1083	8.8510

Table 4. Regressions for the Henderson and Pabis model ($M_R = (a) \exp(-kt)$).

Fruits		k	a	n	c	R²	RMSE	χ2	MBE	MPE
pineapple	1x1x1	0.0069	1.0037	-	-	0.985	0.00052	-0.0006	-0.0045	-8.6598
	1x1x2.5	0.0076	1.117	-	-	0.980	0.00265	-0.0031	0.0086	-3.5396
	sphere	0.0027	1.115	-	-	0.944	0.03280	-0.0382	0.1757	-73.827
avocado	1x1x1	0.0070	1.4179	-	-	0.947	0.02283	-0.0266	0.0506	-3.4628
	1x1x2.5	0.0059	1.463	-	-	0.953	0.03151	-0.0367	0.0918	-16.4503
	sphere	0.0055	1.316	-	-	0.908	0.01443	-0.0168	0.01337	-0.6117
kiwi	1x1x1	0.0089	1.2596	-	-	0.955	0.00923	-0.0109	0.0234	-14.1932
	1x1x2.5	0.0081	1.296	-	-	0.946	0.01337	-0.0158	0.01767	-1.2819
	sphere	0.0067	1.282	-	-	0.963	0.01285	-0.01518	0.01455	-17.9026

Table 5. Regressions for the logarithmic model.

Fruits		k	a	n	c	R²	RMSE	χ2	MBE	MPE
pineapple	1x1x1	0.015	0.944	-	-0.43	0.973	0.00038	-0.0004	-0.00075	-14.6425
	1x1x2.5	0.013	0.901	-	-0.027	0.981	0.00623	-0.0079	0.07277	-73.5226
	sphere	0.009	0.911	-	-0.043	0.961	0.00183	-0.0023	-0.00416	-8.4672
avocado	1x1x1	0.013	1.113	-	-0.013	0.966	0.06895	-0.0878	-0.2185	62.4314
	1x1x2.5	0.015	1.105	-	-0.017	0.976	0.01213	-0.01544	-0.0676	15.3346
	sphere	0.021	1.085	-	-0.018	0.959	0.20440	-0.2602	-0.3879	78.9746
kiwi	1x1x1	0.011	1.125	-	-0.017	0.947	0.01647	-0.0214	-0.0896	39.5625
	1x1x2.5	0.010	1.133	-	-0.019	0.952	0.02385	-0.0310	-0.1130	39.7571
	sphere	0.017	1.097	-	-0.034	0.935	0.13415	-0.1744	-0.3065	81.3499

The higher the values of the EF and R, the better the goodness of the fit. The lower the values of the RMSE, χ^2 and MBE, the better the goodness of the fit. The results have shown that highest values of EF and r and the lowest RMSE, χ^2 and MBE values could be obtained with the statistically fitted model of Modified Page Model.

Equation 5 is solved in order to determine the speed of diffusion. Table 1 provides the change of diffusion coefficient according to the geometric shape of fruits. An examination of the table shows that diffusion coefficient is higher in fruits sliced in 1 x 1 x 1 dimension. Results are in harmony with the data obtained in the literature (36, 37).

Table 6. Variation of the diffusion coefficient with the geometric shape of the fruits.

Fruits	geometric shapes	Diffusion Coefficients (m²/s)
Pineapple	1x1x1	1.654×10^{-8}
	1x1x2.5	1.140×10^{-8}
	sphere	9.100×10^{-9}
Avocado	1x1x1	9.380×10^{-9}
	1x1x2.5	8.110×10^{-9}
	sphere	1.540×10^{-8}
Kiwi	1x1x1	1.190×10^{-8}
	1x1x2.5	9.128×10^{-9}
	sphere	1.650×10^{-8}

Experiments conducted in infrared dryer
In an infrared dryer, the time-moisture content of pineapple, kiwi, and avocado at different sizes was examined and presented in figures.
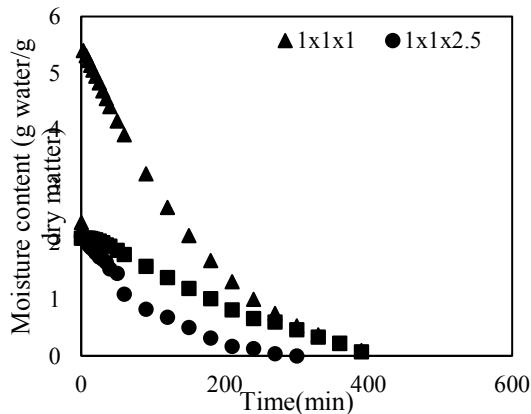

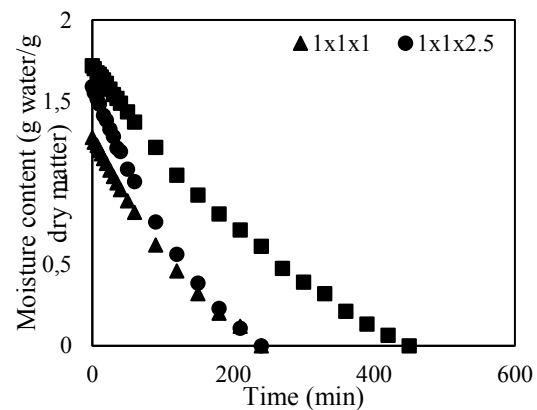**Figure 7.** Variation in moisture content as a function of drying time (pineapple fruit)

Figure 8. Variation in mois ture content as a function of drying time (kiwi fruit)
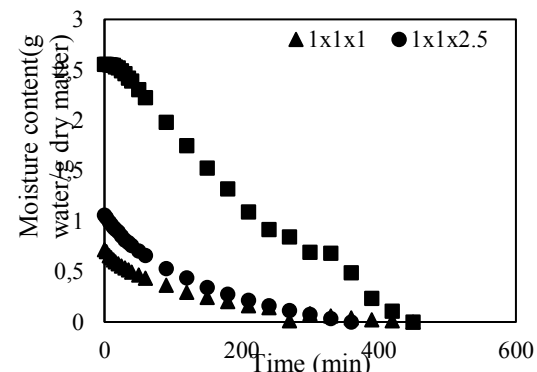

Figure 9. Variation in moisture content as a function of drying time (avocado fruit)

The experiments conducted in infrared dryer showed that fruits sliced in 1x1x1 dimensions dried faster. Only the experiment conducted

for pineapple showed deviations in the fruits sliced in 1x1x1 dimensions. It is believed that this situation was caused by experimental errors.

Ascorbic acid (vitamin C) content of dried fruits

Prior to drying process, the Vitamin C values found in pineapple, avocado and kiwi were 485, 75 and 1002 mg/kg, respectively. After the drying process, Vitamin C values were found as 187.0, 25.9 and 385.4 mg/kg, respectively. These results show that during drying process 60-65% of vitamin C is lost.

CONCLUSIONS

The impact of parameters in the drying process of fruits is discussed and explained with the findings. At the end of this study, the following conclusions can be reached:

1. The effective parameter in both straight flow and infrared drying of fruits is temperature. If the temperature is increased, drying period can be shortened. Temperatures under 50 $^{\circ}$C are not suitable for drying. In the study, drying period can be extended. Again, drying at temperatures above 70 $^{\circ}$C causes change of color and the fruit tends to be baked and then carbonated; thus, it is not recommended.

2. The impact of air velocity on the drying of fruits is not as much as temperature as, during drying, the external shell of the fruit can show excessive resistance against drying, which, in turn, makes the diffusion of moisture more difficult. Air velocity is effective at drying processes where moisture is accumulated especially at external section, meaning at fixed velocity zone. Diffusion is more effective than convection while drying fruits; thus, keeping air velocity low is essential in terms of cost.

3. Among the examined fruits, pineapple and kiwi are very rich in terms of Vitamin C. At the end of the experiments, ascorbic acid amount of pineapple, kiwi and avocado was found as 485, 1002 and 75 mg/kg, respectively. After the drying process, Vitamin C values were determined as 187.0, 25.9 and 385.4 mg/kg. These results show that during drying process 60-65% of Vitamin C is lost.

4. Five different drying models (Modified Page model, Page model, Henderson and Pabis model, Lewis model, and Logarithmic model) were used in order to define the theoretical model which gives the best approach to experimental values. For fruits in different geometric shapes dried at 55 $^{\circ}$C and 1.5 m/s air velocity, it can be said that Modified Page equation provides relatively good results in determining drying behavior. In addition, in all drying models it has been observed that drying coefficient (k), which is an essential

parameter, reduced as the shape grew larger. This is an indicator that drying will be faster when the size of the fruit becomes smaller.

5. It has been observed that diffusion coefficient was larger for fruits sliced in 1x1x1 dimension. The results are in harmony with the values given in the literature.

ACKNOWLEDGMENTS

REFERENCES

1. Kowalski SJ, Mierzwa D, Stasiak M. Ultrasound-assisted convective drying of apples at different process conditions. Drying Technology. 2016 Nov 11;35(8): 939-47.

2. Maskan M, Drying, shrinkage and rehydration characteristics of kiwifruits during hot air and microwave drying. Journal of Food Engineering. 2001;48(2): 177-82.

3. Gürlek G, Akdemir Ö, Güngör A, Gıda Kurutulmasında Isı Pompalı Kurutucuların Kullanımı ve Elma Kurutmada Uygulanması. Pamukkale Üniversitesi Müh. Bilim Dergisi. 2015; 21(9): 398-403.

4. Demiray E, Tülek Y. Kurutma İşleminin Kırmızı Biberdeki Renk Maddelerine Etkisi. Gıda Teknolojileri Elektronik Dergisi. 2012; 7(3): 1-10.

5. Cemeroğlu B. Kurutma teknolojisi. Meyve ve sebze işleme teknolojisi. Gıda Teknolojisi Derneği, 1986; Yayın no:6, Böl: 9, Ankara.

6. Geankoplis CJ. Transport process and unit operations. Allyn and Bacon, Inc., Boston, 1983; 508-657.

7. Alibaş İ. İnce Tabaka Mango Dilimlerinin Mikrodalga Tekniği ile Kurutulması, Uludağ Üniversitesi Ziraat Fakültesi Anadolu Tarım Bilimleri Dergisi. 2015; 30: 99-109.

8. Can A. Kurutma koşullarında biyolojik ürünler içinden nem transportunun kinetiği. Mühendis ve Makine Dergisi. 2000; 33: 392, 9–12.

9. Demir F, Ozcan M. Chemical and technological properties of rose (Rosa canina L.) fruits grown wild in Turkey. Journal of Food Engineering. 2001; 47: 333-6.

10. Avhad MR, Marchetti JM. Mathematical modelling of the drying kinetics of Hass

avocado seeds. Industrial Crops and Products. 2016; 91: 76–87.

11. Perea-Flores MJ, Garibay-Febles V, Chanona-Pérez JJ, Calderón-Domínguez G, Méndez-Méndez JV, Palacios-González E, Gutiérrez-López GF. Mathematical modelling of castor oil seeds (Ricinus communis) drying kinetics in fluidized bed at high temperatures. Ind. Crops Prod. 2012; 38: 64–71.

12. Kaya A, Aydın O, Kolaylı S. Effect of different drying conditions on the vitamin C (ascorbic acid) content of Hayward kiwifruits (Actinidia deliciosa Planch). Food and Bioproducts Processing. 2010; 88(2): 165-73.

13. Arabhosseini A, Huisman W, Van Boxtel A, Müller J. Food and Agriculture Organization of the United Nations Statistics Division. http://faostat3.fao.org/browse/Q/QC/E.

14. Rodríguez O, Gomes W, Rodrigues S, Fernandes FAN. Effect of acoustically assisted treatments on vitamins, antioxidant activity, organic acids and drying kinetics of pineapple, Ultrasonics Sonochemistry. 2017;35: 92–102.

15. Altendorf, S. 2019. Major tropical fruits market review 2018. Rome, FAO

16. Dreher ML, Davenport AJ. Hass avocado composition and potential health effects. Crit Rev Food Science Nutrition. 2013 May;53 (7): 738–50.

17. Pieterse Z, Jerling J, Oosthuizen W. Avocados (monosaturated fatty acids),weight loss and serum lipids. South Afr. Avocado Growers Assoc. Yearbook, 2003; 26: 65–71.

18. Fernandes FAN, Oliveira VS, Gomes WF, Rodrigues S. Degradation kinetics of vitamin E during ultrasound application and the adjustment in avocado purée by tocopherol acetate addition. LWT Food Sci. Technol. 2016; 69: 342– 7.

19. Dantas D, Pasquali, MA, Cavalcanti-Mata M, Duarte ME, Lisboa HM. Influence of spray drying conditions on the properties of avocado powder drink, Food Chemistry. 2018; 266: 284-91.

20. Avhad MR, Marchetti JM. Mathematical modelling of the drying kinetics of Hass avocado seeds. Industrial Crops and Products. 2016; 91: 76-87.

21. Özen E. Farklı Kurutma Teknikleri İle Domatesin Kurutulması. Yüksek Lisans Tezi, Fırat Üniversitesi Fen Bilimleri Enstitüsü, 2017.

22. Erentürk S, Gulapoglu MS, Gultekin S. The effects of cutting and drying medium on the

vitamin C content of rosehip during drying. Journal of Food Engineering. 2005; 68: 513-8.

23. Wang Z, Sun J, Chen F, Liao X, Hu X. Mathematical modelling on thin layer microwave drying of apple pomace with and without hot air predrying. Journal of Food Engineering. 2007; 80: 536-44.

24. Doymaz I, Pala M. The effects of dipping pretreatments on air-drying rates of the seedless grapes. Journal of Food Engineering. 2002; 52: 413-7.

25. Yaldiz O, Ertekin C, Uzun HI. Mathematical modeling of thin layer solar drying of sultana grapes. Energy. 2001; 26: 457-65.

26. Midilli A, Kucuk H, Yapar Z. A new model for single-layer drying. Drying technology. 2002; 20: 1503-13.

27. Yağcioglu A, Değirmencioglu A, Çağatay F. Drying characteristic of laurel leaves under different conditions, in: Proceedings of the 7th international congress on agricultural mechanization and energy. Faculty of Agriculture, Cukurova University, Adana, Turkey, 1999;565-9.

28. Kalender M. Makine Sıva Alçısının İnce Tabaka Infrared Kuruma Kinetiği. Karakteristiği ve Modellenmesi Fırat Üniv. Mühendislik Bilimleri Dergisi. 2017; 29(1): 285-91.

29. Yoğurtçu H. Determination of Drying Kinetics of Tunceli Garlic with Microwave Drying Technique, Tarım Bilimleri Dergisi, 2016; 22: 237-48.

30. Karataş M, Arslan N. Flow behaviours of cellulose and carboxymethyl cellulose from grapefruit peel. Food Hydrocolloids. 2016; 58: 235-45.

31. Sacilik K, Keskin R, Elicin AK. Mathematical modeling of solar tunnel drying of thin layer organic tomato. Journal of Food Eng. 2006; 73: 231-8.

32. Liu Q, Bakker-Arkema FW. Stochastic modelling of grain drying: Part 2. Model development. Journal of Agricultural Engineering Research. 1997; 66: 275–80.

33. Crank J, The mathematics of diffusion. Oxford University Press. OX,UK, 1975.

34. Doymaz İ, Evaluation of some thin-layer drying models of persimmon slices (Diospyoskaki L.) Energy Conversion Management. 2012 April; 56: 199-205.

35. Aboltins A, Upitis A, Experimental and Theoretical Investigation of Agricultural Material Drying Process Engineering for Rural Development. 2012; 24.

36. Dissa A, Desmorieux H, Degraeve P, Bathiebo J, Koulidiati J. Impact of Fruit Ripeness on Physicochemical Properties and Convective Drying Characteristics of Kent Mango (Mangifera indica L. cv. 'Kent'). International Journal of Food Engineering, 2011; 7(3). doi:10.2202/1556-3758.2126. ISSN: 1556-3758.

37. Türk Toğrul İ, Pehlivan D, Modelling of drying kinetics of single apricot Journal of Food Engineering, 2003; 58(1): 23-32.

Study on Desulfurization of Light Gas Oil Using Ionic Liquids Assisted with Ultrasonication

Mohammad F. Abid[a,*] ✉ iD **, Luma H. Mahmood**[b] ✉ iD

[a,*] Department of Medical Instrumentation Engineering, Al-Hikma University College, Iraq.
[b] Department of Chemical Engineering, University of Technology, Iraq.

Abstract: The present work aimed to investigate the feasibility of sulfur extraction from real light gas oil using different types of inorganic ionic liquids (ILs) assisted by ultrasonic waves in a continuous flow setup. Experimental results showed that within 30 min, 66% of sulfur was removed under mild conditions using 10 wt%NaOH assisted by ultrasonic waves. We found that ultrasonic waves not only facilitated the sulfur removal but also it improves gas oil properties by decreasing density and viscosity while cetane number (CN) showed a different trend. The authors presented a correlation of solute selectivity as a function of sulfur mole fraction.

Cite this: Abid MF, Mahmood LH. Study on Desulfurization of Light Gas Oil Using Ionic Liquids Assisted with Ultrasonication. JOTCSB. 2020; 3(1): 19-28.

*Corresponding author: E-mail: 80005@uotechnology.edu.iq.

INTRODUCTION

Desulfurization (DS) of petroleum middle distillates using an efficient cost-effective process is one of the main goals of modern oil refineries. Desulfurization methods mainly cover adsorptive desulfurization (ADS), extractive desulfurization (EDS), oxidative desulfurization ODS), hydrodesulfurization (HDS), biodesulfurization (BDS), and desulfurization by ionic liquids. Though the HDS technique is considered useful in lowering sulfur concentrations in petroleum middle distillates, some sulfur compounds such as dibenzothiophene and its derivatives are less responsive to this operation. Moreover, deep HDS required highly severe pressure and temperature accompanied by higher costs (1). The key is how to select proper adsorbents which cover molecular sieves, activated carbon, ion-exchange resin, and activated carbon fibers (2) to realize the desulfurization process. Jochen *et al*. (3) suggested that EDS with ILs is a good alternate for deep HDS of diesel oil. Duarte *et al*. (4) reported that despite

the significant advantages provided by the use of ultrasound, in the last years, few studies related to its direct application are available in the petroleum industry. Shafeghat *et al.* (5) used ODS assisted by ultrasonic waves to remove sulfur from gas oil and gasoline.

The ILs have withdrawn remarkable interest as extractive materials for DS of middle distillates (6-8), or as an end-step operation for the HDS process (9). Many consider ILs as green chemical solvents with unique physical and chemical properties, like insignificant vapor pressure, high thermochemical stability, and readily be recycled. Moreover, they have high relevance with sulfur-compounds (S-compounds), in particular with aromatic S-components, and have good miscibility with middle distillates, which nominates ILs as good extracting agents for desulfurization of fuels (10-11). Many organic ILs are expensive, for example, imidazolium-based ILs (12). Fluoride based ILs can absorb humidity and produce toxic hydrogen fluoride known

as a defective product (13-14). In the current study, we investigated the feasibility of usage effective-cost ILs in a continuous process for extractive desulfurization (EDS) of gas oil under ambient conditions. Another objective was to study the equilibrium behavior of sulfur compounds in studied ternary mixtures.

MATERIALS AND METHODS

Materials
The authors purchased high purity chemicals of sodium chloride (99.0 wt% min), sodium hydroxide (> 98%), and calcium hydroxide (> 96%) from Sigma Aldrich, India. We ordered hydrochloric acid (36%) from Merck, Germany. We also obtained light gas oil from Al-Daura Oil Refinery, Baghdad. Table 1 lists the specifications of real gas oil.

Table 1. Properties of real light gas oil feed (Al-Daura Oil Refinery, Baghdad).

Property	Method of analysis	Value
API@15.6 ^{0}C	ASTM D1298	40.1
Sp.gr @ 15.6 ^{0}C	ASTM D1298	0.8246
Sulfur content (ppm)	ASTM D 5623	2140
Cetane number	ASTM D 7170	51.2
Distilled (vol.%) in crude oil	ASTM D 86	17.1
I.B.P (^{o}C)	ASTM 6352	195
E.B.P (^{o}C)	ASTM 6352	322

Experimental procedure for selectivity and partition coefficient
The authors installed a batch setup to predict the behavior of selectivity and the partition coefficient for the studied systems. Mixtures of ternary systems components (IL + S-compound + oil) in the immiscible region were mixed in a 50 mL glass vessel immersed in a water bath and connected to a recirculation Chiller type Accel 250 LC from Thermo Scientific, to control the vessel temperature at (25±1 °C). The mixtures were agitated using a magnetic stirrer for 1 h, and then let stabilize for a minimum of 2 h. We considered that these periods being enough to attain a proper equilibrium between constituents producing a pure yellow aqueous solution. Then, we used syringes to obtain samples from each layer of the mixture. GC was used to measure the weight fractions of oil and sulfur compounds, and we tabulated the results.

Experimental setup for continuous operation
Of each ionic material (sodium hydroxide, calcium hydroxide, and hydrochloric acid), three different concentrations (5, 10, and 15 wt%) were prepared separately in 100- mL glass beakers. 50 mL of gas oil was taken in an Erlenmeyer flask and added to each prepared ionic aqueous solution in a 250 mL-cylindrical glass Flask (V1), respectively. The mixing was applied at 300 rpm by an electric mixer type (IKA RW 20, Cole-Parmer). We selected this mixing speed as the optimum value after a series of mixing

experiments. We then transferred the mixture to another 250- mL glass cylindrical vessel (V2), which contained an ultrasonic generator (Model VCX-750, vibra-cell, Sonics) whose probe immersed in the mixture. Table 2 lists the characteristics of the ultrasonic probe. We kept the temperature of the sonication vessel at 40 °C because, above this temperature, extraction of S-compounds becomes increasingly more inadequate (15). The authors sonicated the mixture for 30 min with a 4 min of a break between sequential ultrasonic periods of 5 min. As the sonication process continued, samples for sulfur determination were drawn periodically by a syringe. We neglected the influence of sampling on mixture volume because of the small sample amounts (≤ 1.0 mL per sample). After ultrasonic periods of 30 min, we conveyed the mixture to a funnel of liquid-liquid separation (S1) to let separate the denser layer from the oil light layer. Then the oil light layer was transmitted to a 250-mL glass beaker (V3) where a neutralizing agent was added (if required). We then utilized a pH meter type (On-line pH meter Model Excel 25PH/mV/ISL) to monitor the pH of the solution in V3. We transferred the neutralized solution to a high-speed centrifuge type (Centrisart® D-16C, Sartorius Company). The authors analyzed the lighter stream (desulfurized gas oil) for the concentration of total sulfur utilizing a sulfur analyzer type (XOS, Model: Sindie OTG). We rechecked the analysis result with GC. Figure 1 shows a plot of the experimental setup in **Figure 1**.
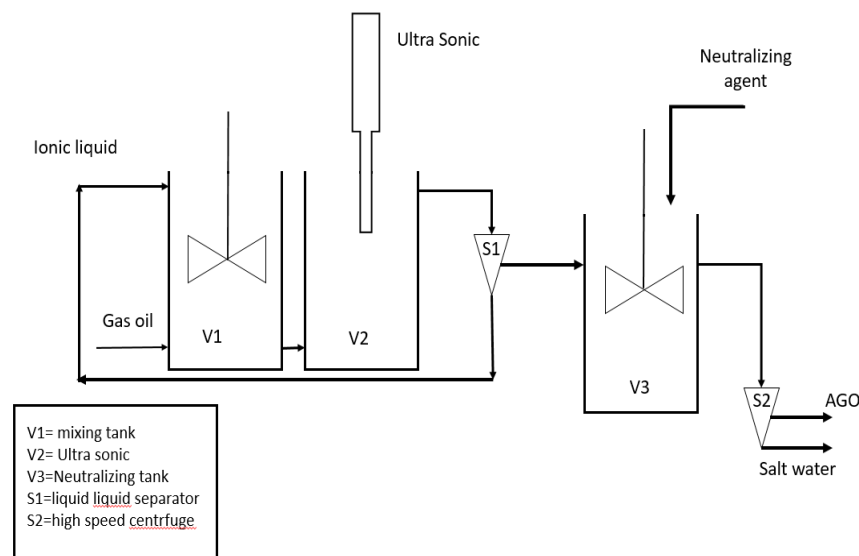
Figure 1: Experimental setup of the continuous extractive desulfurization process.

Table 2: Specifications of the ultrasound probe.

Characteristics	Values
Power Output	750 Watts
Frequency	20 kHz
Standard Probe Size	Diameter: 13 mm ; Length:136 mm
Probe Material	Titanium Alloy Ti-6Al- 4V
Processing Capacity	10 mL – 350 mL

Method of analysis

The fractions of the samples in the ternary systems were measured by GC type ta3000 (AMETEK® Process Instruments), equipped with a column SPB-1 SULFUR 30 m x 0.32 mm ID 4.0 µm phase and flame ionization detector (FID). We utilized the analyzer of sulfur type (XOS, Model: Sindie OTG) to measure the total sulfur content of gas oil before and after the EDS process. (FTIR) records were carried out in the 400–4000 cm^{-1} range, using the IR Affinity-1, Shimadzu analyzer. Cetane number (CN) of gas oil was measured using near infrared diesel oil cetane number testing instrument model FDW-0371, China. Gas oil density was measured using **density meter model DDM 2909** from Rudolph Research Analytical, USA. Initial and end boiling points of gas oil were determined using distillation tester, model: PT-D1401-255 from Genius Laboratories, China.
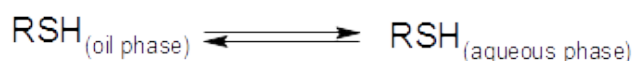
THEORETICAL ASPECTS

It is scientifically apparent that ultrasonic irradiation can effectively improve the reaction yield in chemical synthesis. The result is cavitation when mechanical vibrations generate into the liquid as ultrasonic waves. When one subjects liquids to high-intensity ultrasonic waves, it creates acoustic cavitation. This phenomenon is the formation and succeeding violent collapsing of cavitation bubbles, creating shock waves, preparing a great set of conditions for chemical reactions, and increasing the chemical reactivity in the system. During this process, short-term, localized hotspots can form. The violent collapse of each bubble causes locally high temperatures (up to 5000 K), high pressure (up to 1000 atm), and drastic liquid jets. This micro-environment, with extreme local conditions, is suitable for the creation of active intermediates permitting the reaction to progress rapidly. Moreover, ultrasonic waves may assist in increasing the formation of lighter sulfur-molecules due to the breakage of heavier ones (16).

The basis of the mechanism of extraction is on the allocation law, which states that if a liquid layer consists of two immiscible components, it subjoins a material which is dissolvable in both layers. Then the material doled out between the two layers so that the ratio of loading in one solvent to the loading in the other solvent stays stable at a stable temperature. It is supposed that the molecular structure of the material is identical in both solvents. The distribution or partition coefficient (k_d) is presented by Eq. 1 (17).

$$k_d = \frac{x_s^1}{x_s^2}$$

(Eq. 1)

where x_s^1 the S-compound loading in phase 1 (i.e., IL-rich phase) and x_s^2 is the loading of S-compound in phase 2 (i.e., hydrocarbon-rich phase). As a comparative approach, the allocation parameter may be estimated equivalent to the ratio of the solubility of S-compound in the two layers. One dissolves organic sulfur components readily in the polar solvents; moreover the solvents having consanguinity for the sulfur compounds being extra beneficial in their extraction. So, we have utilized this method in the present work by applying various solvent systems at identical conditions (*e.g.,* temperature and processing time). Heinrich and Kasztelan (18) reported that mercaptans and sulfides form the main proportions of S-compounds that are present in the lighter middle distillates of petroleum. One assumes that the S-compound is soluble in the oil phase. Eqns may represent the distribution of an S-compound between an oil phase and an aqueous inorganic ionic solution. (2 – 3) following:

$$RSH_{(oil\ phase)} \rightleftarrows RSH_{(aqueous\ phase)}$$

$$RSH_{(aqueous\ phase)} \rightleftarrows RSH^-_{(aqueous\ phase)}$$

(Eq. 2)(Eq. 3).

Equilibrium 1 depends on the solubility of the S-compound in the aqueous phase and in the oil phase. Equilibrium 2 depends on the ionization constant of the S-compound and on the

concentration of free hydroxide of water. Cabo (19) presented Eq. 4 to correlate to the solute distribution ratio, k_d, and selectivity, S,

$$S = \frac{x_s^1}{x_s^2} \cdot \frac{x_0^2}{x_0^1} \qquad \text{(Eq. 4)}$$

Where x_0^2 and x_0^1 are mole fractions of gas oil in phase 2 and phase 1 respectively.

RESULTS AND DISCUSSION

Selectivity and partition coefficient
It is a well-known fact that the solute partition coefficient, k_d, and selectivity, S, are linked to the amount of solvent required for the separation (k_d) and to the number of required steps to achieve it (selectivity). Thus, they are key parameters to decide the appropriateness of a solvent as an extracting material. The k_d and S values obtained for the Liquid-liquid Equilibria data of studied systems *i.e.*, [10% NaOH + S-compound+ Oil], and [10% Ca(OH)₂+ S-compound + Oil] respectively are shown in Tables 3 and 4. We drew these values versus the sulfur compound's molar fraction in the oil-rich phase in **Figure 2**(a-b). The trends of S are qualitatively similar for both ILs. This figure demonstrates that the separation of S-compound from light gas oil with these ILs is favorable in terms of solubility and selectivity, especially at low mole fractions of S-compound. When we obtain higher values of k_d and S for the studied mixtures, we obtain a more efficient separation of S-compound from the oil (20).

Table 3: Experimental data of (10% NaOH + S-compound + Oil) system.

Ionic liquid-rich phase			Oil-rich phase			k_d	S
x_1^1	x_2^1	x_3^1	x_1^2	x_2^2	x_3^2		
0.893	0.00	0.107	0.00	0.00	1.00		
0.754	0.15	0.096	0.00	0.029	0.971	5.17	52.29
0.677	0.24	0.083	0.00	0.062	0.938	3.87	43.73
0.514	0.412	0.074	0.00	0.157	0.823	2.62	29.13
0.416	0.525	0.059	0.00	0.263	0.737	1.99	24.85
0.34	0.618	0.042	0.00	0.404	0.596	1.529	21.69
0.311	0.646	0.043	0.00	0.471	0.529	1.37	16.85
0.275	0.68	0.045	0.00	0.558	0.442	1.21	11.88

Table 4: Experimental data of (10% Ca(OH)₂ + S-compound + Oil) system.

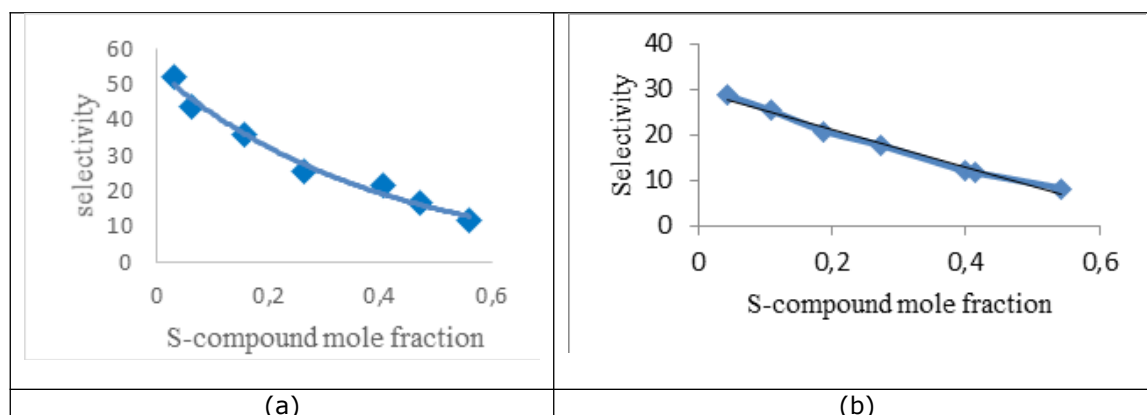| Ionic liquid-rich phase			Oil-rich phase			k_d	S
x_1^1	x_2^1	x_3^1	x_1^2	x_2^2	x_3^2		
0.941	0.00	0.059	0.00	0.00	1.00		
0.863	0.078	0.059	0.00	0.044	0.956	1.77	28.68
0.759	0.182	0.059	0.00	0.108	0.892	1.68	25.39
0.663	0.279	0.058	0.00	0.187	0.813	1.49	20.88
0.578	0.367	0.055	0.00	0.272	0.728	1.34	17.73
0.489	0.454	0.057	0.00	0.400	0.600	1.139	11.98
0.47	0.473	0.057	0.00	0.415	0.585	1.134	11.64
0.404	0.541	0.055	0.00	0.544	0.456	0.99	8.21

Figure 2: Variation of selectivity against mole fraction of sulfur for mixtures of (a) 10% NaOH+(S-compound)+oil, and (b) 10% Ca(OH)$_2$+(S-compound)+oil.

Based on the experimental data, related correlation selectivity *vs.* sulfur mole fraction in studied ternary mixtures can represent using StatPlus 6.5.1.0 software by Eqs (5-6).
for the mixture (10% NaOH +(S-compound)+ oil):

$S = 53.969\ e^{-2.552x\_s}$, $R^2 = 0.9813$ (Eq. 5)
for the mixture (10%Ca(OH)$_2$+(S-compound)+ oil):

$S = 29.573 - 41.878\ x_s$, $R^2 = 0.986$ (Eq. 6)

Effect of IL type

Figure 3 illustrates the variation of sulfur removal against processing time using various types of ILs. It is apparent that for using 10% NaOH as the processing time continues to increase from 5, 10,

15, and 20 min, the sulfur removal (%) rises steadily from 20, 35, 52, and 62%. However, as the processing time increased further from 20, 25 to 30 min, sulfur removal showed slower increases from 52, 62, and 65. Therefore, the operating system may establish an equilibrium state at the final stages of the process. For 10% Ca(OH)$_2$ and 1N HCl, the same behaviors were shown in **Figure 3** of sulfur removal versus processing time but at lower values of sulfur removals. So the aqueous solution of NaOH offers a higher affinity towards sulfur compounds. We attained the lower sulfur removal with 1N HCl. It is likely due to the high tartness, which is not an appropriate medium for the allocation of aromatic sulfur combinations, which demands an alkaline environment rather than an acidic environment (21).
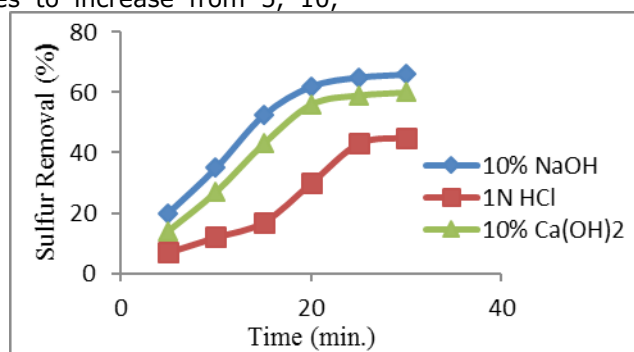

Figure 3: Variation of sulfur removal against processing time using various types of IL.

Figure 4 (a-b) shows the higher percentage of sulfur removal achieved by processing gas oil with different types of ionic liquid assisted with or without ultrasonic waves, respectively. As shown, sulfur removal (%) promoted in the arrangement of using 1N HCl < 10% Ca(OH)$_2$ < 10% NaOH. We may attribute this trend to that NaOH aqueous solution has larger consanguinity for the S-compounds in the oil distillates. It is possibly because of the acidic

feature of the specific sulfur components such as mercaptans, which easily disseminates from the oil phase inside the alkaline stratum of NaOH and turns into sulfides. In the same way, the high EDS output gained with Ca(OH)$_2$ may also be elucidated fundamentally, as mentioned above. Although the alkalinity feature of Ca(OH)$_2$ is minimal than that of NaOH, yet, DS effectiveness of Ca(OH)$_2$ is analogous with that of NaOH, which proposes that calcium

endures some grade of chemical charisma to mercaptans and sulfides. A comparison between **Figure 4**a and **4**b depicts the noticeable effect of ultrasonic waves on EDS of gas oil. The increase in sulfur removal due to the sonication of the IL/gas oil mixture was 24.2% for 10% NaOH, 10% Ca(OH)$_2$,

and 1N HCl, respectively. It may be due to the ultrasonic waves which assist in increasing the formation of lighter sulfur-molecules due to bond breaking of heavier molecules facilitating the extraction of S-compound by ILs (16).

(a)	(b)

Figure 4: Variation of sulfur removal (%) against type of ionic liquid (a) assisted with ultrasonic waves; (b) without ultrasonic waves.

Effect of IL concentration

Figure 5 shows a variation of sulfur removal against processing time using a different concentration of NaOH solution. As can be seen in the figure, for all concentrations a steep increase in sulfur removal occurred at the early stages of processing. One may attribute to the high rate of extraction, which is positively affected by the high concentration of sulfur compound existed at these stages, creating a higher driving force of sulfur concentration between the two layers. After then, as sulfur concentration decreased

continuously, the extraction rate decreased correspondingly until a pseudo-equilibrium state was established at the final stage of the process *i.e.* at 25-30 min. **Figure 5** indicates that sulfur removal was positively affected by the concentration of NaOH. However, **Figure 5** depicts that there is an optimum concentration of IL which may be used to attain the best sulfur removal, after which any increase in NaOH concentration would be only costly (19).
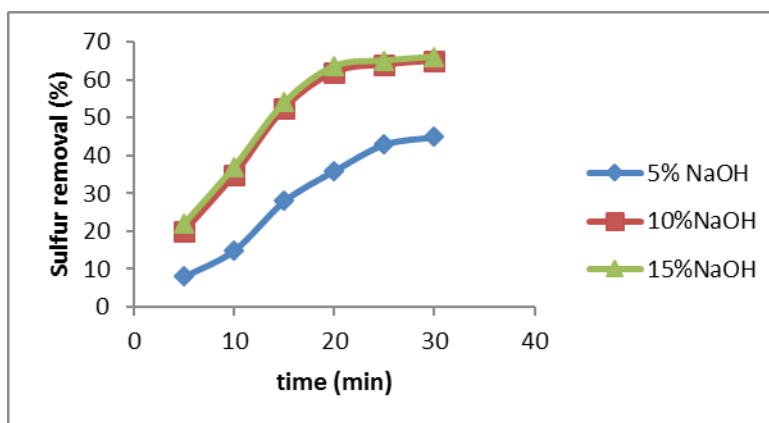

Figure 5: Influence of the concentration of aqueous %NaOH sulfur removal at various processing times.

Effect of ultrasonic process on gas oil properties

Slamet *et al.* (22) considered viscosity as the last significant diesel fuel characteristic due to its influence on the system of pressurized combustion. Stavarache *et al.* (23) reported that a method to upgrade the physical properties of diesel fuel (like

viscosity) is to employ external power convey irradiation with various origins (ultrasound, microwaves, infrared waves, ultraviolet, *etc.*). Some of these power origins are capable of adjusting at the micro-molecular grade the chemical framework of the fuel, with instant effect on its physical characteristics. Therefore it is of importance to

investigate the influence of the sonication process on some properties (*e.g.,* viscosity, CN, API) of produced gas oil. Table 5 lists the measured properties of gas oil before and after the sonication process. As can be observed, both viscosity and the specific gravity of gas oil decreased while CN shows a different trend. This behavior is due to the collapsing of cavitation bubbles, creating shock waves, increasing the chemical reactivity in the

system. Moreover, ultrasonic waves assist in increasing the formation of lighter sulfur-containing molecules due to the breakage of heavier ones. We know that the value of CN links to the period desired for fuel to fire after injection to the burning engine. The more the CN, the speedier is the firing time. This CN rises with long straight carbon chains produced by breaking the branched carbon chain due to high-intensity ultrasonic waves (24).

Table 5. Measured properties of real light gas oil feed before and after sonication process.

Property	Values	
	Before	After
API@15.6 ^{0}C	40.1	42
Sp.gr @ 15.6 ^{0}C	0.8246	0.8155
Viscosity, SSU	32.3	31
Cetane number	51.2	54.8
I.B.P (^{o}C)	165	157
E.B.P (^{o}C)	290	281

Effect of mixing speed

To investigate the influence of mixing speed on stabilization time and S-compound extraction, we performed a series of experiments, Figure 7 shows these trends. As can be seen in Figure 7, that a percentage extraction of S-compound of 37, 65. 4 and 66 % is attained by a stirring speed of 200, 300,

and 350 rpm respectively with a stabilization time of 2 hours. The positive impact of stirring speed on percentage extraction of the S-compound may attribute to the reduction in the mass transfer limitations because of the turbulence action. However, from the power savings point of view, a stirring speed of 300 rpm is selected for operation.
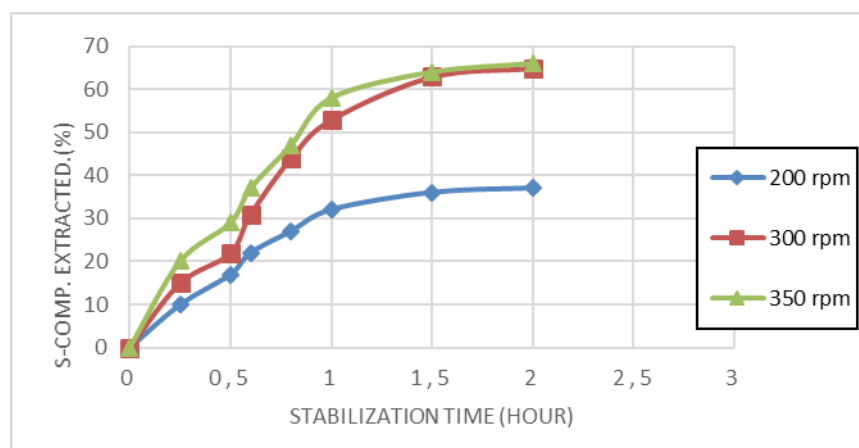

Figure 7: Effect of mixing speed on stabilization time and S-compound extraction.

FTIR spectra

Figure 7 shows the FTIR spectra of the real light gas oil, and **Figure 7** (lower spectrum) points out the existence of mercaptans by a notable band in the domain of 2360 cm^{-1} because of the S-H. A less thick moderate band at 1380 cm^{-1} points out the S=O asymmetrical oscillation, which bears a sign of the sulfonyl chlorides, sulfonates, sulfones or sulfoxides. A broad band at 3420 cm^{-1} demonstrates the

existence of the HN or HO, which matches to the bond related to sulfonamides. The FTIR spectrum of the gas oil cured with NaOH (10%) is in **Figure 7** (upper spectrum). The visions indicate that bands in that domain showing mercaptans S-H (at 2370 cm^{-1}) and S=O (at 1380 cm^{-1}) are impotent in strength in (upper spectrum) comparable to the spectrum of the actual sample.
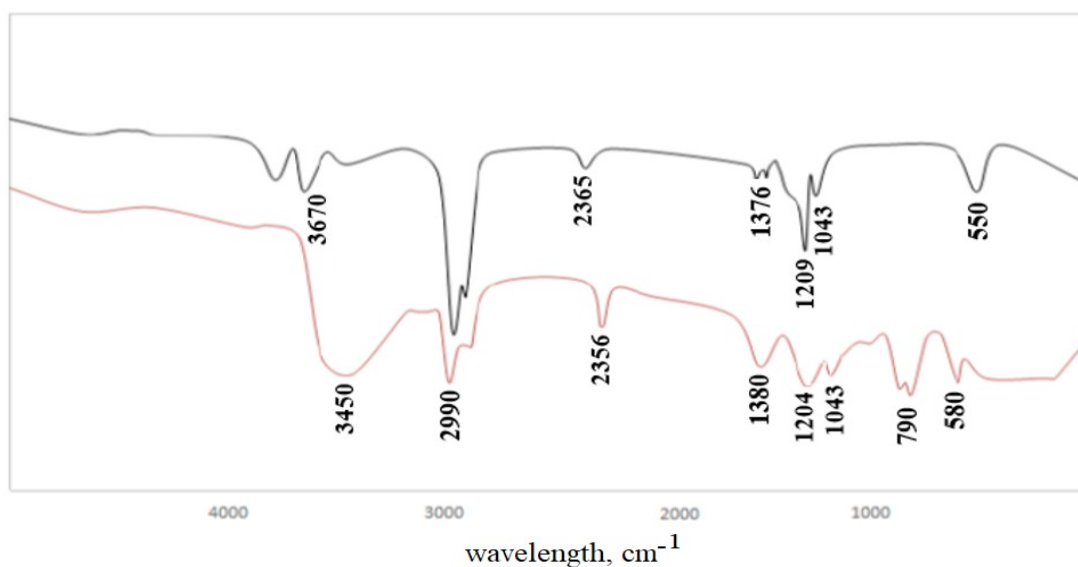
Figure 7: FTIR spectrum of gaseous oil before treatment with 10% NaOH (bottom) and after EDS with 10% NaOH (top).

EDS mechanism

Figure. 8 displays the probable pathway of sulfur extracted by NaOH**.** Since the DS of divalent sulfur of 4,6-DMDBT compounds follows the nucleophilic extraction mechanism, the extraction step began with the nucleophilic attack of electron density rich in the sulfur atom (4,6-DMDBT) to the electrophilic character of ⁻OH in NaOH. The (CH3)3C–O_ was then re-joined with the hydroxyl and the 4,6-DMDBT sulfoxide formed.

Figure 8: EDS mechanism of S-compound by NaOH.

Economic Aspects

In the present study, we designed the suggested extractive desulfurization process to operate in a continuous production mode under ambient conditions (see Fig. 1). The consumption rate of ionic liquids and sulfur removal from gas oil are considered the main factors affecting the process feasibility. Due to the density difference between gas oil (ρ_{oil} = 0.82 g/cm^3) and that of ionic liquids (ρ_{NaOH} = 1.11 g/cm^3 and ρ_{HCl} = 1.02 g/cm^3), separator (S1) worked with a reasonable efficiency which enabling ionic liquids to recycle to the mixing tank (V1). Consumption rates for 10% NaOH and 1N HCl per 100 g of desulfurized gas oil (DGO) produced were estimated by 0.97 and 2.87 g respectively which equivalent to a percentage loss of (~ 1%) for NaOH and (~ 3%) for HCl with desulfurization of gas oil up to 66.0 and 60.0% obtained by an ultrasonication process using ILs of 10% NaOH and 1 N HCl, respectively.

CONCLUSION

The present work aimed to investigate the feasibility of sulfur extraction from light gas oil using different types of cost-effective inorganic ionic liquids (ILs) such as NaOH, Ca(OH)$_2$, and HCl, assisted by ultrasonic waves at irradiated power of 750W with 20 kHz, in continuous operation under mild conditions of temperature and pressure. The study of

the equilibrium system for the selected ternary mixtures showed that solute selectivity was inversely related to solute mole fraction. We have found that, within 30 min, 10 wt% NaOH offered a higher sulfur removal of 66% and 50% with and without sonication process, respectively. Moreover, we showed that ultrasonic waves not only increased the sulfur removal by 24.2% but it also improved gas oil properties by decreasing density and viscosity by 1.30 and 4.02% respectively while cetane number (CN) was increased by 6.3%.

ACKNOWLEDGEMENT

REFERENCES

1. Song C. An overview of new approaches to deep desulfurization for ultra-clean gasoline, diesel fuel and jet fuel. Catalysis Today. 2003 Nov;86(1–4):211–63.

2. Gawande P, Meghe D, Kaware J. Desulphurization Techniques for Liquid Fuel A Review. International Journal of Engineering Technology Management and Applied Sciences. 2014;2(7):121–7.

3. Eßer J, Wasserscheid P, Jess A. Deep desulfurization of oil refinery streams by extraction with ionic liquids. Green Chem. 2004;6(7):316–22.

4. Duarte FA, Mello P de A, Bizzi CA, Nunes MAG, Moreira EM, Alencar MS, et al. Sulfur removal from hydrotreated petroleum fractions using ultrasound-assisted oxidative desulfurization process. Fuel. 2011 Jun;90(6):2158–64.

5. Shafeghat A, Ghaedian M, Mehrabi M. Desulfurization of gas oil by using ultrasonic waves. Journal of Petroleum Research. 2015;24(80):85–95.

6. Mochizuki Y, Sugawara K. Removal of Organic Sulfur from Hydrocarbon Resources Using Ionic Liquids. Energy Fuels. 2008 Sep 17;22(5):3303–7.

7. Li F, Liu Y, Sun Z, Chen L, Zhao D, Liu R, et al. Deep Extractive Desulfurization of Gasoline with x Et 3 NHCl·FeCl 3 Ionic Liquids. Energy Fuels. 2010 Aug 19;24(8):4285–9.

8. Hansmeier AR, Meindersma GW, de Haan AB. Desulfurization and denitrogenation of gasoline and diesel fuels by means of ionic liquids. Green Chem. 2011;13(7):1907.

9. Nie Y, Li C, Meng H, Wang Z. N,N-dialkylimidazolium dialkylphosphate ionic liquids: Their extractive performance for thiophene series compounds from fuel oils versus the length of alkyl group. Fuel Processing Technology. 2008 Oct;89(10):978–83.

10. Jian-long W, Zhao D, Zhou E, Dong Z. Desulfurization of gasoline by extraction with N-alkyl-pyridinium-based ionic liquids. Journal of Fuel Chemistry and Technology. 2007 Jun;35(3):293–6.

11. Kędra-Królik K, Fabrice M, Jaubert J-N. Extraction of Thiophene or Pyridine from n-Heptane Using Ionic Liquids. Gasoline and Diesel Desulfurization. Ind Eng Chem Res. 2011 Feb 16;50(4):2296–306.

12. Liu X, Zhou G, Zhang S, Yu G. Molecular simulations of phosphonium-based ionic liquid. Molecular Simulation. 2010 Jan;36(1):79–86.

13. Varma NR, Ramalingam A, Banerjee T. Experiments, correlations and COSMO-RS predictions for the extraction of benzothiophene from n-hexane using imidazolium-based ionic liquids. Chemical Engineering Journal. 2011 Jan;166(1):30–9.

14. Chen X, Yuan S, Abdeltawab AA, Al-Deyab SS, Zhang J, Yu L, et al. Extractive desulfurization and denitrogenation of fuels using functional acidic ionic liquids. Separation and Purification Technology. 2014 Sep;133:187–93.

15. Afshar A, Hashemi S. Role and effect of temperature on LPG sweetening process. International Journal of Chemical and Molecular Engineering. 2011;5(7):628–30.

16. Mello P de A, Duarte FA, Nunes MAG, Alencar MS, Moreira EM, Korn M, et al. Ultrasound-assisted oxidative process for sulfur removal from petroleum product feedstock. Ultrasonics Sonochemistry. 2009 Aug;16(6):732–6.

17. Shakirullah M, Ahmad I, Ahmad W, Ishaq M. DESULPHURIZATION STUDY OF PETROLEUM PRODUCTS THROUGH EXTRACTION WITH AQUEOUS IONIC LIQUIDS. J Chil Chem Soc [Internet]. 2010 Jun [cited 2020 Apr 13];55(2). Available from: http://www.scielo.cl/scielo.php?script=sci_arttext&pid=S0717-97072010000200007&lng=en&nrm=iso&tlng=en

18. Heinrich G, Kasztelan S. Hydrotreating, in Petroleum Refining. Leprince P, editor. Paris: Institut Français Du Pétrole Publications; 2001.

19. Cabo B. Desulfurization of fuels with ionic liquids by extraction and oxidative extraction processes [PhD Thesis]. [Compostela]: University of Santiago de Compostela; 2013.

20. Robbins L, Cusack R. Liquid-Liquid Extraction Operations and Equipment. In: Green D, Maloney J, editors. Perry's Chemical Engineering Handbook. New York: McGraw-Hill Company; 1997.

21. Leerdam RC van. Anaerobic degradation of methanethiol in a process for Liquefied Petroleum Gas (LPG) biodesulfurization. 198 p.

22. Supriyadi S, Purwanto P, Dwi anggoro D, Hermawan. Enhancing Biodiesel from Kemiri Sunan Oil Manufacturing using Ultrasonics. Hadiyanto, Sudarno, Maryono, editors. E3S Web Conf. 2018;31:02014.

23. Stavarache C, Vinatoru M, Maeda Y. Ultrasonic versus silent methylation of vegetable oils. Ultrasonics Sonochemistry. 2006 Jul;13(5):401–7.

24. Chen D, Sharma SK, Mudhoo A. Handbook on applications of ultrasound sonochemistry for sustainability [Internet]. Boca Raton, Fla.: CRC Press; 2012 [cited 2020 Apr 13]. Available from: https://www.taylorfrancis.com/books/97814398420 72

RESEARCH ARTICLE

Application of Discrete-Time Controllers to A Pilot Scale Packed Distillation Column

Semin Altuntaş [a, b] ✉ iD **, Hale Hapoğlu** [a] ✉ iD
a* Chemical Engineering Department, Ankara University, Ankara, Turkey.
b Provincial Directorate of Environment and Urbanization, Samsun, Turkey.

Abstract: The process involved is a pilot scale packed distillation column that separates a mixture of methanol and water. The performances of two discrete-time controllers that different parameter tuning techniques were used for each of them were examined in the face of the set point tracking of the overhead product composition. The success of the discrete-time controllers was assessed by means of the rise time and integral of the square error (ISE) criteria. A discrete-time proportional-integral (PI) controller with two terms was obtained by using the velocity form of controller law. For this controller, firstly the proportional sensitivity term (K_c) was determined by creating a root locus diagram. The other term that corresponded to the sampling time (T_s) to integral time constant (τ_I) ratio multiplied by half of K_c value was then chosen by replacing the closed-loop poles to the appropriate location in unit circle of z-plane. The most successful proposed controller action was obtained with K_c of 0.95 and integral time constant of 2.375 min according to rise time of 3.7 min and ISE criteria of 1.08. The discrete-time proportional-integral-derivative (PID) controller with six parameters as P=0.009185, I=0.01835, D=0, N=100, b=1, c=1 that were tuned by using Simulink control design and 1 min sampling time was applied to the process. The same controller performance with six parameters of P=1.164, I=0.5319, D=-0.01481, N=3.783, b=0.1233, c=0.01017 was investigated by choosing 0.5 min sampling time. By comparing all the performances obtained, it can be said that the discrete-time controller with two terms tuned by the suggested approach can easily be applied to obtain the most desired performance.

Cite this: Altuntaş S, Hapoğlu H. Application of Discrete-Time Controllers to A Pilot Scale Packed Distillation Column. JOTCSB. 2020;3(1):29–34.

*Corresponding author. E-mail: seminaltuntas@hotmail.com.

INTRODUCTION

Discrete-time controller accuracy and speed have importance in industrial applications. A compromise is needed between cost and reliability (4). The corresponding controllers are called digital computers. System models are described in certain discrete-time domain, and their parameters are determined by using various methods based on experimental or well-simulated input and output data (2-3). The controlled systems dynamics are determined by the choice of controller parameters which are determined using various methods (1).

Discrete-time controllers are designed to minimize a cost function or to locate closed-loop system poles in the z-plane unit circle. Obtaining a desired closed-loop system response of a controller also minimize indirectly a cost function. A cost effective design based on a closed-loop pole-placement approach was reported for discrete proportional- integral controller (7). For two-degrees-of-freedom (2DOF) PI current controller, an analytical discrete-time pole-placement technique was used (6). By separating a closed-loop system poles as a dominant pole pair and other poles and locating them in z-plane unit circle by targeting a certain distance between each set of poles, a discrete PI-proportional-derivate (PI-PD) controller was designed by Dincel and

Söylemez (2018). This technique is called a dominant pole-placement.

In the present work, two discrete-time controllers were used to track set point of the overhead product composition of a pilot-scale packed distillation column for performance comparison. The two tuning parameters of the proposed discrete PI controller were tuned by observing root locus diagram pole branches for proportional only control and by choosing the three poles location in z-plane according to a performance criteria of the system response with discrete PI controller. The two application performances of discrete-time PID controller (2DOF) that the related six parameters tuned by means of Simulink control design in MATLAB were also examined by choosing the sampling time (T_s) as 1 min and 0.5 min respectively. As can be seen from the Simulink applications, the high value of the sampling time can destabilize the control or will at least result in the deviations of the controlled variable being much larger than necessary. If the chosen sampling time is larger than the real system delay, then a pole-placement based proposed discrete-time controller still produces acceptable set point tracking response.

DISCRETE-TIME CONTROLLERS

Wardle and Hapoglu (1993) proposed a discrete-time transfer function of process without control. This transfer function response to a step increase in control signal was compared (10) with two-film approach model computer simulation that verified (9) by the experimental data (8) obtained from a pilot-scale packed distillation column where methanol water mixture was fed between 1 m and 0.9 m effective packing height in enriching and stripping sections.

The discrete system transfer function (10) without control which relates the deviation form of overhead product molar methanol composition (x_D') and the deviation form of reflux flow rate (L') was given in **Equation (1)**. Where, the T_s value was used as 1 min. The same system discrete transfer function can be written by using T_s of 0.5 min and zero order hold element in **Equation (2)**.

$$\frac{x'_D}{L'} = \frac{0.411\,z + 0.0119}{z^2 - 0.742\,z + 0.0183} \tag{1}$$

$$\frac{x'_D}{L'} = \frac{0.2122\,z - 0.01472}{z^2 - 1.006\,z + 0.1353} \tag{2}$$

The closed-loop system with proportional control transfer function which relates overhead product composition in **Equation (1)** and set point was given in **Equation (3)**.

$$\frac{x'_D}{x'_{SET}} = a$$

$$a = \frac{K_c(0.411\,z + 0.0119)}{(z^2 - 0.742\,z + 0.0183) + K_c(0.411\,z + 0.0119)} \tag{3}$$

Where, x'_{SET} represents the set point value of the overhead product composition in deviation variable form. K_c is the proportional sensitivity (or the gain) of the proportional (P) controller. The characteristic equation of the transfer function given in **Equation (3)** was utilized to create root locus diagram data. The K_c value that locates two desired positive poles far from the edge of the unit circle was chosen to apply as a constant value in **Equation (9)**.

The proposed discrete-time PI controller transfer function was written as **Equation (4)**, because the changes of the manipulated variable are determined by varying two terms. **Equation (7)** is obtained by combining the discrete definition of the coefficients q_0 and q_1 which are given in **Equation (5)** and **Equation (6)** respectively. The velocity form control algorithm is utilized to create the terms in **Equation (5)** and **Equation (6)**. The tuning parameter of A was presented in **Equation (8)**.

$$G_c(z) = \frac{q_0 z - q_1}{z - 1} \tag{4}$$

$$q_0 = K_c + \frac{K_c T_s}{2\tau_I} \tag{5}$$

$$q_1 = \frac{K_c T_s}{2\tau_I} - K_c \tag{6}$$

$$G_c(z) = \frac{(K_c + A)z - (A - K_c)}{z - 1} \tag{7}$$

$$A = \frac{K_c T_s}{2\tau_I} \tag{8}$$

$$G_c(z) = \frac{(0.95 + A)z - (A - 0.95)}{z - 1} \tag{9}$$

Where τ_I is integral time constant which was varied by using different values of A (see **Equation (9)**).

$$ISE = 10^4 \sum_{n=0}^{n=N} T_s(x_{SET} - x_D)_n^2 \tag{10}$$

For controller performance comparison,

integral of the square error (ISE) criteria given in **Equation (10)** was used in discrete domain, where the error (x_{SET}-x_D) is the deviation of the overhead product composition from the set point. The N value is the total number of sampling time step used to reach the final run time.

$$G_c(z) = P(b*x'_{set}) + I*T_s\frac{1}{z-1}(x'_{SET}-x'_D)$$

$$+D\frac{N}{1+N*T_s\frac{1}{z-1}}(c*x'_{SET}-x'_D)$$

$$(11)$$

The second discrete controller was obtained from Simulink Library in MATLAB. This discrete PID controller (2DOF) was presented in **Equation (11)**. Where P, I, D represent proportional, integral, derivative terms respectively. The parameters of b and c are the set point weights. The symbol of N is filter coefficient. The discrete PID controller block parameters was tuned by using Simulink Control Design in MATLAB. By substituting zero for D in **Equation (11)** the discrete PI controller Simulink block was obtained.

RESULTS AND DISCUSSION

The discrete-time transfer function of the packed distillation column without control (10) which relates overhead product molar methanol composition as output and reflux flow rate as inputs was used to capture the closed-loop behavior of the process with proportional only control. The proportional sensitivity (K_c) of the closed-loop transfer function given in **Equation (3)** was varied to determine the poles location in z-plane by using MATLAB (see **Table 1**). Root locus diagram obtained was presented in **Figure 1**. The branches corresponding to the two poles of the proportional only control system begin at the two poles (0.7165 and 0.0255) of the system transfer function without control (These poles are represented by symbols of cross in **Figure 1**).

In **Table 1**, The Kc value was varied by considering the related root locus diagram to determine adequate location for the poles. For non-oscillatory stable case, K_c=0.95 was chosen with two real positive closed-loop poles as 0.2119 and 0.1397.

At all set point tracking applications studied in the present work, an initial step change from 0.969 to 0.978 was introduced. For the proposed discrete-time PI controller parameters identification the K_c value selected from **Table 1** was used in **Equation (7)**. The coefficient of A in **Equation (9)** was selected based on closed-loop pole placement technique by considering the three poles location and the ISE criteria (**Table 2**). For this selection, the controlled variable behaviors versus time were also examined (**Figure 2-4**).
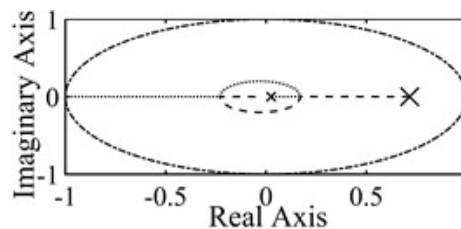

Figure 1: Root locus diagram generated using MATLAB for the closed-loop discrete system with P controller.

Table 1: Poles for the closed-loop discrete system with P controller.

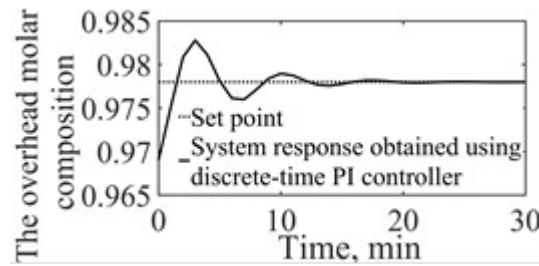| K_c	poles	
1.1	0.1450-0.1019i	0.1450+0.1019i
1.0	0.1655-0.0530i	0.1655+0.0530i
0.98	0.1692-0.0346i	0.1692-0.0346i
(*) 0.95	0.2119	0.1397
0.90	0.2609	0.1112
0.80	0.3285	0.0847
0.009185	0.7124	0.0258

(*) represents the selected poles and K_c

Figure 2: The control of overhead product composition using the proposed discrete-time PI controller with T_s=1.0 min, Kc=0.95, τ_I=0.28 min, A=1.7.

Table 2: Poles for the discrete system with PI controller.

A	Three poles	ISE
1.70	0.3222±0.9953i, 0.0086+0.0000i	79.26
0.70	0.5155±0.6143i, 0.0331+0.0000i	1.41
0.40	0.5683±0.4124i, 0.0504+0.0000i	1.10
(*) 0.20	0.5987±0.1466i, 0.0716+0.0000i	1.08
0.18	0.6016±0.0735i, 0.0748+0.0000i	1.10
0.17	0.6527, 0.5529, 0.0764	1.11
0.16	0.7055, 0.5023, 0.0782	1.13
0.15	0.7400, 0.4700, 0.0800	1.14

The symbol (*) represents the selected A value according to ISE criteria. The values of K_c and T_s are 0.95 and 1 min respectively.

In the cases studied (**Table 2**), with the proposed discrete-time PI controller, the offset problem did not exist. However, the addition of the integral (I) action with A=1.7 (T_s=1.0 min, τ_I=0.28 min) in the discrete controller that includes the previously chosen K_c value of 0.95 caused the oscillatory system response and increased the maximum deviation from the desired value (**Figure 2**). The system response to a change in set point may exhibit less oscillatory behavior with tolerable rise time or non-oscillatory behavior with high rise time as value of A decreases (τ_I value increases).

Figure 3 showed that the A value of 0.15 produced an overdamped response with high rise time of 8.8 min. The best response according to minimum ISE criteria and rise time of 3.7 min was shown in **Figure 4**.
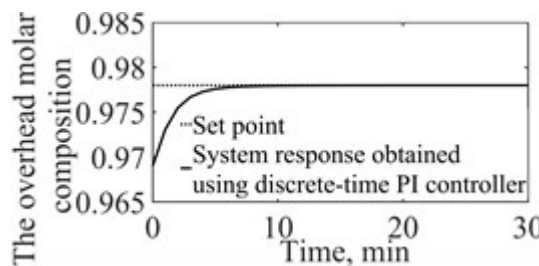

Figure 3: The control of overhead product composition using the proposed discrete-time PI controller with T_s=1.0 min, K_c=0.95, τ_I=3.17 min, A=0.15.

The discrete PID controller (2DOF) which is available in MATLAB/Simulink library was examined when applied to the overhead product composition control of the packed distillation column in the face of a set point change from 0.969 to 0.978. Its six tuning parameters were determined as P=0.009185, I=0.01835, D=0, N=100, b=1, c=1 using Simulink control design by using T_s of 1 min. It was noted that the PID controller given in **Equation (11)** converted to the PI control action by substituting zero (D=0) for the last term. The overhead product composition set point tracking with this controller was shown in **Figure 5**. This control action performance according to ISE criteria was evaluated as 15.89. This response with 169 min rise time exhibited sluggishness.
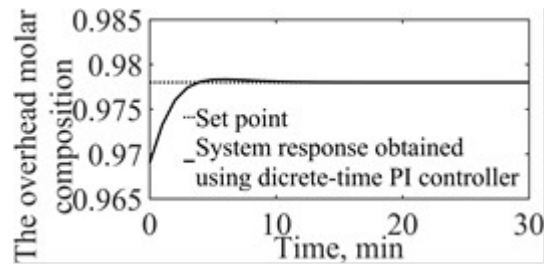
Figure 4: The control of overhead product composition using the proposed discrete-time PI controller with T_s=1.0 min, K_c=0.95, τ_I=2.375min, A=0.2.
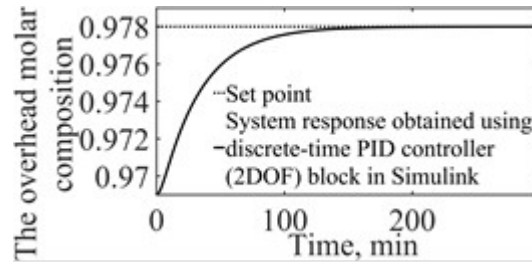

Figure 5: The closed-loop response of overhead product composition with the discrete-time PID controller (2DOF) that is available in MATLAB/ Simulink library.

By using T_s of 0.5 min and the system transfer function in **Equation (2)**, the discrete PID controller (2DOF) parameters were also determined as P=1.164, I=0.5319, D=-0.01481, N=3.783, b=0.1233, c=0.01017 using Simulink control design. The closed-loop system response obtained was illustrated in **Figure 6**. This set point tracking response obtained with the discrete PID controller (2DOF) performed with the ISE criteria of 3.68 and the rise time of 8 min. A decrease in T_s from 1 min to 0.5 min revealed 95.27 % and 76.84 % decreases in the ISE and in the rise

time values respectively.

In the present work, the theoretical cost-effective performance of the proposed controller was shown. This enhanced the economic performance of the modeled pilot-scale packed distillation column. Therefore, it is worth to use the discrete-time controller and evaluate the cost reduction of an industrial-scale packed column with the discrete-time controllers.
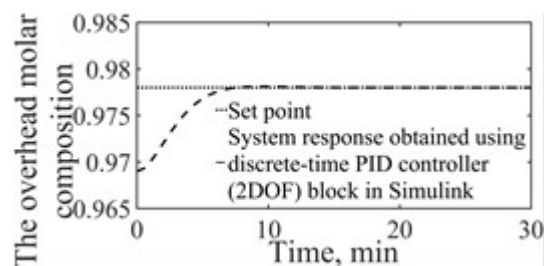

Figure 6: The control of overhead product composition using the discrete-time PID controller (2DOF) Simulink block that its parameters tuned as P=1.164, I=0.5319, D=-0.01481, N=3.783, b=0.1233, c=0.01017.

CONCLUSION

Clearly, the proposed discrete PI controller with the technique applied based on root locus search and pole-placement approach has a desired influence upon the set-point tracking performance of the overhead product composition of a packed distillation column. The discrete proposed PI controller exhibited much better performance than the one

obtained using the discrete PID (2DOF) controller in MATLAB/Simulink library. This controller can be recommended for relatively high sampling time applications.

The advantages of the proposed controller used in the present work were low rise time, low settling time and very smooth transient response. It was shown that the desired level of performance was guaranteed by using suitable tuning technique based on pole-

placement for the proposed controller parameters. There is currently a considerable need for the controller as described in the present work to be implemented on a full-scale industrial packed distillation column.

REFERENCES

1. Aldemir A, Hapoglu H. Comparison of PID tuning methods for wireless temperature control. JOURNAL OF POLYTECHNIC-POLITEKNIK DERGISI. 2016;19(1):9–19.

2. Altuntaş S, Hapoğlu H, Ertunç S, Alpbaz M. Experimental Self-Tuning Proportional Integral Derivative pH Control: Application to a Bioprocess. Acta Phys Pol A. 2017 Sep;132(3–II):1006–9.

3. Camcıoğlu Ş, Özyurt B, Doğan İC, Hapoğlu H. Application of response surface methodology as a new PID tuning method in an electrocoagulation process control case. Water Science and Technology. 2017 Dec 13;76(12):3410–27.

4. E. N. Desyatirikova, V. I. Akimov, D. V. Sysoev, V. E. Mager, L. V. Chernenkaya. Selection of Controller Settings in Digital Control Systems. In: 2019 IEEE Conference of Russian Young Researchers in Electrical and Electronic Engineering (EIConRus). 2019. p. 474–7.

5. Dincel E, Söylemez MT. Digital PI-PD controller design for arbitrary order systems: Dominant pole placement approach. ISA Transactions. 2018 Aug;79:189–201.

6. Hinkkanen M, Awan HAA, Qu Z, Tuovinen T, Briz F. Current Control for Synchronous Motor Drives: Direct Discrete-Time Pole-Placement Design. IEEE Transactions on Industry Applications. 2016;52(2):1530–41.

7. Khan PF, Sengottuvel S, Patel R, Gireesan K, Baskaran R, Mani A. Design and Implementation of a Discrete-Time Proportional Integral (PI) Controller for the Temperature Control of a Heating Pad. SLAS TECHNOLOGY: Translating Life Sciences Innovation. 2018 Dec;23(6):614–23.

8. Steiner L, Barendreght HP, Hartland S. Concentration profiles in a packed distillation column. Chemical Engineering Science. 1978;33(3):255–62.

9. Wardle H, Hapoglu H. On the solution of models of binary and multicomponent packed distillation columns using orthogonal collocation on finite elements. Chemical engineering research & design. 1994;

10. Wardle H, Hapoglu H. On the solution of models of binary and multicomponent packed distillation columns using orthogonal collocation on finite elements. In: Chemical engineering research & design. Zurich, Switzerland: Acta Press; 1993. p. 431–4.